

CaaX-motif adjacent residues control G protein prenylation under suboptimal conditions

Short title: Molecular underpinnings of G protein Gamma ($G\gamma$) prenylation

Mithila Tennakoon^{1,3,4}, Waruna Thotamune^{1,3,4}, John L. Payton², Ajith Karunarathne^{1,3,4*}

¹ Department of Chemistry, Saint Louis University, Saint Louis, MO 63103, USA

² Department of Chemistry, Kenyon College, Gambier, Ohio 43022, USA

³ Department of Chemistry and Biochemistry, The University of Toledo, Toledo, OH 43606, USA

⁴ Institute for Drug and Biotherapeutic Innovation, Saint Louis University, Saint Louis, MO 63103, USA

*Corresponding author: wkaranarathne@slu.edu

Abstract

Prenylation is a universal and irreversible post-translational modification that supports membrane interactions of proteins involved in various cellular processes, including migration, proliferation, and survival. Thus, dysregulation of prenylation contributes to multiple disorders, including cancers, vascular diseases, and neurodegenerative diseases. During prenylation, prenyltransferase enzymes tether metabolically produced isoprenoid lipids to proteins via a thioether linkage. Pharmacological inhibition of the lipid synthesis pathway by statins has long been a therapeutic approach to control hyperlipidemia. Building on our previous finding that statins inhibit membrane association of G protein γ ($G\gamma$) in a subtype-dependent manner, we investigated the molecular reasoning for this differential. We examined the prenylation efficacy of carboxy terminus (Ct) mutated $G\gamma$ in cells exposed to Fluvastatin and prenyl transferase inhibitors and monitored the subcellular localization of fluorescently tagged $G\gamma$ subunits and their mutants using live-cell confocal imaging. Reversible optogenetic unmasking-masking of Ct residues was used to probe their contribution to the prenylation process and membrane interactions of the prenylated proteins. Our findings suggest that specific Ct residues regulate membrane interactions of the $G\gamma$ polypeptide statin sensitivity, and prenylation efficacy. Our results also show that a few hydrophobic and charged residues at the Ct are crucial determinants of a protein's prenylation ability, especially under suboptimal conditions. Given the cell and tissue-specific expression of different $G\gamma$ subtypes, our findings explain how and why statins differentially perturb heterotrimeric G protein signaling in specific cells and tissues. Our results may provide molecular reasoning for repurposing statins as Ras oncogene inhibitors and the failure of using prenyltransferase inhibitors in cancer treatment.

Keywords

GPCR; G proteins, prenylation; prenyltransferases; statin; cholesterol; mevalonate pathway; HMG-CoA reductase; optogenetics

1. Introduction

Post-translational lipid modifications, including N-myristoylation, palmitoylation, prenylation, glycosylphosphatidylinositol (GPI) anchor addition, and cholesterol attachment, expand the functional and structural diversity of the eukaryotic proteome (1, 2). The chemical and physical properties, activities, and cellular distribution of proteins are significantly modified by the covalent attachment of a non-peptidic hydrophobic moiety to a protein. This results in the interaction of post-translationally modified proteins with cellular membranes and facilitates multiple cellular signaling pathways (2). Protein prenylation has been studied extensively due to its significance in the proper cellular activity of numerous proteins. Prenylation includes both farnesylation and geranylgeranylation and is an irreversible covalent post-translational modification found in all eukaryotic cells. These modification reactions are catalyzed by three prenyltransferase enzymes. Farnesyltransferase (FTase) or geranylgeranyltransferase type 1 (GGTase-I) catalyzes the covalent attachment of a single farnesyl (15 carbon) or geranylgeranyl (20 carbon) isoprenoid group, respectively, to a cysteine residue located in a C-terminal (Ct) consensus sequence commonly known as the "CaaX box", in which "C" is cysteine, "a" generally represents an aliphatic amino acid, and the "X" residue determines which isoprenoid is attached to the protein target (3). Geranylgeranyltransferase type 2 (GGTase-II or Rab geranylgeranyltransferase) catalyzes the addition of two geranylgeranyl groups to two cysteine residues in sequences such as CXC or CCXX close to the Ct of Rab proteins (4, 5).

Inhibition of hepatic cholesterol biosynthesis is widely accepted to mitigate cardiovascular diseases such as Coronary Heart Disease (CHD) (6). This is achieved by inhibiting the rate-limiting enzyme, HMG-CoA reductase, of the cholesterol biosynthesis (mevalonate) pathway (7). Commonly called statins, these HMG-CoA reductase inhibitors interfere with the synthesis of intermediate products of the cholesterol biosynthesis pathway, such as isoprenoids (8, 9). Isoprenoids are precursor lipids for synthesizing cholesterol and other lipid derivatives, including farnesyl, geranyl, and geranylgeranyl pyrophosphates, squalene, dolichol, and ubiquinone. The above mentioned pyrophosphates are required for the prenylation of small and heterotrimeric G proteins (10-12). Our previous work revealed the influence of statin usage on G $\beta\gamma$ and, consequently heterotrimeric G-protein signaling due to the inhibition of G γ prenylation (13). We showed that not only do statins disrupt G γ prenylation, G γ farnesylation is more susceptible to this inhibition than geranylgeranylation (13).

The essential role of farnesylation in modulating the oncogenic activity of Ras function led to the discovery of farnesyltransferase inhibitors (FTIs) such as Tipifarnib and Lonafarnib (14-16). The combined anti-tumor activity and low toxicity of these FTIs observed in animal models directed clinical trials to use FTIs as anti-tumor drugs (17). However, discouraging results have been observed due to the alternative prenylation exhibited in KRas and NRas (to a lesser extent), where the effect of FTIs is evaded by the activity of GGTase-I (17). Therefore, a thorough understanding of the molecular mechanism of prenylation and post-prenylation processing is crucial to develop more efficient drugs for tumor progression prevention. Given the antiproliferative effects of statins, repurposing them as anticancer drugs can also be considered (12). Observations from *in vitro* and *in vivo* pre-clinical studies and clinical studies report the anticancer effects of statins (18). Statins have shown antiproliferative effects in various cancers by primarily inhibiting the synthesis of cholesterol and its metabolites (19-21), which result in

tumor growth suppression, induction of apoptosis and autophagy, inhibition of cell migration and invasion, and inhibition of angiogenesis (22-24). Therefore, it is believed that statins can influence patient survival and cancer recurrence (25). Several pleiotropic effects, including antioxidant, anti-inflammatory, and immune-modulatory properties, are also associated with statin usage, which can be causing their antiproliferative properties (26). *In vitro* studies conducted in a broad range of cancer cell lines present evidence for the anticancer properties of statins (18). For instance, Simvastatin exhibited anticancer potential in several cancer types, such as hepatoma, breast cancer, endometrial cancer, osteosarcoma, and lung adenocarcinoma (22, 27-30). Additionally, Atorvastatin exhibited anticancer effects on ovarian cancer in a study conducted using Hey and SKOV3 cells (23). Anticancer efficacy of statins has also been demonstrated during *in vivo* pre-clinical studies using xenograft animal models. For example, a xenograft mouse study showed the anti-tumor effect of Pitavastatin on glioblastoma (31). This evidence suggests the potential use of statins and prenyltransferase inhibitors as anticancer drugs in a combinatorial therapy approach. G $\beta\gamma$ interacts with many effectors, regulates a wide range of physiological functions, and thus has been established as a major signaling regulator (32). Although prenylation is crucial for not only G $\beta\gamma$ function but also GPCR-G protein signaling, molecular details are lacking on how statins influence G γ prenylation.

Our data suggest that the peptide adjacent to the prenyl-Cys (pre-CaaX) region differentially regulates G protein γ sensitivity to prenylation inhibitors. Further, the described behaviors of G protein polypeptides and prenyl pyrophosphates will show how pharmacological agents, including statins and prenyltransferase inhibitors influence these proteins. Finally, our findings will further help utilize these molecular interactions to open new therapeutic windows to target G proteins-associated diseases.

3. RESULTS

3.1 G γ subtypes show differential sensitivities to statin-mediated perturbation of the plasma membrane localization

Prenylated G γ s primarily stay bound to the plasma membrane when they are in the G $\alpha\beta\gamma$ heterotrimer (Fig. 1A-Control) (33). G γ s also show a minor presence at endomembranes, likely due to heterotrimer shuttling (34, 35), activities of Guanine nucleotide Exchange Factors (GEFs) that activate minor amounts of heterotrimers (36), or interactions with endomembrane-residing GPCRs (37). Throughout this manuscript, we examined G γ or G γ mutant localization in HeLa cells by transfecting only fluorescently tagged G γ subunits and relied on endogenous G α and G β subunits to govern the subcellular distributions. When G γ s are not prenylated, they show a cytosolic distribution due to the failure of the membrane anchoring (13, 38). We have previously shown that while statin treatment significantly reduces the membrane anchoring of several G γ types, indicated by their presence in the cytosol (Fig. 1- G γ 1 in control vs. Flu), other G γ types showed a disruption of membrane binding only partially. We observed that the partial inhibition is indicated by the absence of G γ localization at endomembranes and reduced plasma membrane localization. Further, these G γ s show minor to significant cytosolic distribution, and the extent depended on the G γ subtype (ex: Fig. 1- G γ 2 in control vs. Flu) (13). G γ s with more cytosolic presence upon statin exposure also exhibit a nuclear localization as indicated by homogenous cell interior fluorescence. However, the molecular underpinnings of these G γ subtype-dependent differential de-localizations of G γ upon statin exposure were unclear. Though it is generally accepted that the CaaX motif determines the type of prenylation (farnesylation or geranylgeranylation) of a G protein, it has also been suggested that amino acids beyond this motif, extending up to 25 C-terminal residues, are also involved (39). To understand whether the observed statin-induced protein localization signatures of different G γ types are exclusively dependent on their type of prenylation, we examined Fluvastatin (20 μ M)-induced prenylation inhibition of the entire G γ family (Fig. 1A-Flu). In our previous study, we tested a few statins, i.e., Fluvastatin, Lovastatin, and Atorvastatin, for their ability to disrupt membrane localization of G γ and, thereby, G $\beta\gamma$ -mediated downstream signaling. Of these three statins, Fluvastatin exhibited the highest efficiency in perturbing G γ localization and G $\beta\gamma$ signaling (13). Considering all the optimized conditions, we used Fluvastatin to examine statin-induced G γ de-localization in this study. Three G γ types reported to be exclusively farnesylated (G γ 1, 9, and 11) showed near-complete sensitivity to Fluvastatin, indicated by the cytosolic and nuclear distribution of YFP-G γ while they also lacked plasma membrane distribution (Fig. 1A-Flu). We have previously shown that partial sensitivity to statins is characterized by the complete lack of G γ at endomembranes, while their presence on the plasma membrane is detectable (13). Interestingly, geranylgeranylated G γ types (G γ 2, 3, 4, 5, 7, 8, 10, 12, and 13) showed two distinct phenotypes. G γ 2, 3, 4, 7, 8, and 12 showed partial sensitivity, while unexpectedly, the rest G γ types (G γ 5, 10, and 13) showed a near-complete sensitivity to statins (Fig. 1A-Flu). This raised the question of whether these G γ s (5, 10, and 13) are geranylgeranylated as predicted. To

examine their exact type of prenylation, we exposed cells expressing each G γ subtype to farnesyl transferase inhibitor (FTI), Tipifarnib - 1 μ M or geranylgeranyl transferase inhibitor (GGTI), GGTI286 - 10 μ M. As expected, G γ 1, 9, and 11 showed a completely inhibited phenotype upon FTI exposure (Fig. 1A- FTI). This also indicated that the remaining G γ members are geranylgeranylated. Interestingly these FTI insensitive G γ s showed varying sensitivities to GGTI, from moderate to high. Particularly G γ 5, 10 and 13 showed near-complete inhibition while G γ 2, 3, 4, 7, 8 and 12 showed only a partial prenylation inhibition (Fig. 1A-GGTI).

Since the visual inspection of G γ membrane localization inhibition provides only a qualitative estimate of membrane anchorage inhibition, we employed mobilities of G γ , or lack thereof, as a measure of prenylation. Compared to prenylated G γ , G γ with impaired prenylation is expected to have faster mobilities due to reduced membrane interactions (34). To evaluate the mobilities of YFP-tagged G γ , we examined recovery after photobleaching of half-cell fluorescence and calculated the time to half maximum fluorescence recovery, which we termed mobility half-time ($t_{1/2}$) (Table 1) (35). When proteins are not membrane bound, they move faster since they are cytosolic. However, when only a fraction of the protein population is membrane-anchored, the mobility represents an ensemble movement of both membrane-bound and cytosolic species. Regardless of the G γ subtype and their type of prenylation, mobility $t_{1/2}$ values of all the control (untreated) G γ s in the heterotrimer were nearly similar, with the average $t_{1/2}$ of 97 ± 4 s (one-way ANOVA: $F_{11,174} = 1.763$, $p = 0.064$) (Fig. 1B). This indicates that G γ s in control cells are in the heterotrimeric form, making their mobility rates G γ subtype independent (34). When examined, the mobility $t_{1/2}$ of Fluvastatin exposed G γ 1, 9, and 11 were nearly similar and 11 ± 5 s, 9 ± 5 s, and 9 ± 5 s, respectively (one-way ANOVA: $F_{2,33} = 0.615$, $p = 0.547$) (Fig. 1C- G γ 1, 9 and 11). These mobility $t_{1/2}$ values are comparable with the mobility $t_{1/2}$ of the prenylation-deficient G γ 3_{C72A} mutant (10 ± 5 s) that showed a complete cytosolic distribution (one-way ANOVA: $F_{3,84} = 0.406$, $p = 0.749$) (Fig. 1C-G γ 3_{C72A}). When G γ 3 expressing cells were exposed to Fluvastatin, the observed mobility $t_{1/2}$ (55 ± 13 s) falls between that of prenylated G γ 3 in control (101 ± 14 s) and the completely cytosolic G γ 3_{C72A} mutant (10 ± 5 s) (Fig. 1C- G γ 3). This mobility rate of Fluvastatin-exposed G γ 3 suggests the presence of both cytosolic and membrane-bound G γ s, indicating partial disruption of membrane anchorage. Compared to untreated conditions, the ~2-fold reduction in G γ 3 mobility $t_{1/2}$ upon Fluvastatin treatment also signifies the increased cytosolic fraction of G γ 3. Similarly, GGTI exposed G γ 3 also showed an intermediate mobility $t_{1/2}$ (43 ± 9 s) (Fig. 1E- G γ 3), indicating partial geranylgeranylation inhibition. FTI exposed G γ 3 showed a mobility $t_{1/2}$ (98 ± 15 s) that is not significantly different from control G γ 3 (101 ± 14 s) (one-way ANOVA: $F_{1,24} = 0.250$, $p = 0.621$), suggesting that FTI cannot inhibit the activity of geranylgeranyl transferase-I (Fig. 1D- G γ 3). Upon FTI treatment, the mobility $t_{1/2}$ of farnesylation-sensitive G γ s (G γ 1, 9, and 11) are significantly reduced (~9-10 s) while that of geranylgeranylation-sensitive G γ s remained nearly unchanged, confirming the exclusive farnesylation-sensitivities of these G γ s (Fig. 1D). Nevertheless, upon exposing cells to GGTI, only geranylgeranylation-sensitive G γ s showed a significant reduction in mobility $t_{1/2}$ (Fig. 1E), while their mobility was unaffected upon FTI exposure (Fig. 1D). However, GGTI-induced prenylation inhibition sensitivity of geranylgeranylation-sensitive G γ s also showed a wide range from near complete (as in G γ 5, 10, and 13) to partial (as in G γ 2, 3, 4, 7, 8, and 12).

3.2 Statin-induced G γ delocalization to the cytosol is prenylation-type independent

Our previous work has established that G γ subunits such as γ 9, γ 1, and γ 11 show faster translocation with $t_{1/2}$ of a few seconds and greater magnitudes. They were identified as low membrane affinity G γ s. Conversely, G γ with larger translocation $t_{1/2}$ values and lower magnitudes, including G γ 2, γ 3, and γ 4, are considered to be high membrane affinity G γ s (40). Interestingly, when examined, the fastest translocating G γ 9 and the slowest translocating G γ 3 also exhibited two distinct sensitivities to Fluvastatin-induced membrane anchorage inhibition; G γ 9 with near-complete cytosolic distribution and G γ 3 with partial cytosolic distribution (Fig. 1A and C) (13). To quantitatively define these two classifications (complete cytosolic vs partial cytosolic), we assigned G γ s with 0-24 s mobility $t_{1/2}$ values as complete cytosolic and G γ with 25-60 s mobility $t_{1/2}$ as partial cytosolic. According to this classification, upon Fluvastatin exposure, ~100% of the G γ 9 cells showed a prominently increased cytosolic fluorescence due to cytosolic G γ , while the fraction of cells with partial cytosolic distribution was nearly zero and insignificant (Fig. 2A, 2B and Table 3, G γ 9-WT). Interestingly, ~99% of G γ 3 cells showed partial inhibition of membrane binding while near-complete inhibition was inconsequential with Fluvastatin treatment (Fig. 2A, 2B and Table 3, G γ 3-WT). To examine the contribution of the CaaX sequence in determining the degree of statin-induced retardation of membrane binding, we compared CaaX motif mutants of G γ 9 and G γ 3 with their corresponding wild types. Similar to G γ 9-WT, when exposed to Fluvastatin, ~99% of cells expressing a G γ 9 mutant with the CaaX sequence of G γ 3 (G γ 9_{CALL}) exhibited near-complete cytosolic distribution indicating complete disruption of membrane binding (Fig. 2A, 2B and Table 3, G γ 9_{CALL}). However, the FTI and GGTI sensitivities of the G γ 9_{CALL} mutant showed that it is geranylgeranylated as predicted from its CaaX (CALL) sequence (Fig. 2A, G γ 9_{CALL}). Similarly, the G γ 3 mutant containing the CaaX sequence of G γ 9 (G γ 3_{CHS}) showed a partial disruption of membrane anchoring when cells were exposed to Fluvastatin even though it is farnesylation sensitive (Fig. 2A, G γ 3_{CHS}). This response was prominent in ~97% of the mutant-expressing cells, while only ~3% of the total population exhibited near-complete inhibition of membrane binding (Fig. 2B and Table 3- G γ 3_{CHS}). We also calculated mobility rates of the wild type and two G γ mutants (Fig. 2C and Table 2). Even though switching the CaaX motif convincingly switched the FTI and GGTI sensitivities of G γ 9 and G γ 3, the Fluvastatin sensitivity remained unchanged between the WT controls and the corresponding mutants, implying distinct molecular determinants governing the statin sensitivity of G γ .

3.3 Pre-CaaX sequences of G γ s control their statin sensitivity

Since Fluvastatin-induced membrane binding inhibition profiles of G γ family members were G γ -type dependent, we examined the molecular reasoning for this behavior, especially considering that Fluvastatin sensitivity of G γ is independent of their prenylation type. We have extensively documented that, in addition to prenyl and carboxymethyl modifications on the Ct Cys of G γ , its adjacent pre-CaaX region also controls G $\beta\gamma$ -membrane interactions (40-42). Our previous work showed the crucial involvement of pre-CaaX residues in specific G γ s regulating their membrane affinity (41). Therefore, we examined whether the chemistry of pre-CaaX amino acids also controls the protein's statin sensitivity (Fig. 3A). For this, we computationally determined the hydrophobicity of the Ct polypeptide of G γ only comprising pre-CaaX and CaaX regions (before prenylation), using octanol-water partition coefficient (K_{OW})-based *Log Cavity Energy* (*Log CE*) calculation (please see Methods 2.5) (Fig. 3B, Table S1). It has been shown that the difference between the free energy of cavity formation in the organic and water solvents

indicates a peptide's relative affinity between the two phases and its hydrophobicity (43). All the $\text{G}\gamma$ -derived peptides showed higher positive ΔG values for water (ΔG_W). Interestingly, $\text{G}\gamma 2, 3, 4, 5,$ and 8 exhibited lower but positive ΔG values for octanol (ΔG_O), indicating that they have a higher affinity to the lipid phase (Table S1).

The cavity energy of pre-CaaX+CaaX peptides of $\text{G}\gamma$ indicates that $\text{G}\gamma 4, 3, 2,$ and 8 possess significantly higher stability in lipids compared to $\text{G}\gamma 1, 9,$ and 11 . Interestingly, log CE of pre-CaaX+CaaX of $\text{G}\gamma 10$ and 13 also showed less favorable values for lipids in the same range as $\text{G}\gamma 1, 9,$ and 11 (Fig. 3B, Table S1). These log CE values agree with our unexpected observation that similar to $\text{G}\gamma 1, 9, 11,$ geranylgeranylated $\text{G}\gamma 10, 13$ also possess similar sensitivity to Fluvastatin (Fig. 1 and 3B). This aligns with our hypothesis that unprenylated polypeptide regulates the prenylation efficacy by interacting differentially with membranes where prenylation occurs. Further, the pre-CaaX+CaaX peptides from $\text{G}\gamma 5, 7,$ and 12 that showed log CE values between the above two groups ($\text{G}\gamma 2, 3, 4, 8$ vs. $\text{G}\gamma 1, 9, 11$), also exhibited partial, however, more significant prenylation inhibition than $\text{G}\gamma 2, 3, 4, 8$ upon Fluvastatin, supporting our hypothesis (Fig. 3B and Table S1).

Since these findings suggest the involvement of the pre-CaaX region in regulating $\text{G}\gamma$ -membrane interactions, and different $\text{G}\gamma$ types show distinct sensitivities to statin, regardless of the type of prenylation, we tested the hypothesis that the pre-CaaX region hydrophobicity of $\text{G}\gamma$ polypeptide govern their statin sensitivity. We first examined the influence of exchanging pre-CaaX sequences between $\text{G}\gamma 3$ and $\text{G}\gamma 9$, representative $\text{G}\gamma$ s of the two extremes of $\text{G}\gamma$ membrane affinities (40). We comparatively examined the statin sensitivity of the $\text{G}\gamma 9$ mutant containing the pre-CaaX (PC) of $\text{G}\gamma 3$ ($\text{G}\gamma 9_{\text{G}\gamma 3\text{PC}}$ or **-NPFREKKKFFCLIS**) that we reported previously (41) and a new $\text{G}\gamma 3$ mutant containing the pre-CaaX of $\text{G}\gamma 9$ ($\text{G}\gamma 3_{\text{G}\gamma 9\text{PC}}$ or **-NPFKEKGGCALL**). Interestingly, in the presence of Fluvastatin, cells expressing $\text{G}\gamma 9_{\text{G}\gamma 3\text{PC}}$ exhibited a prominent partial inhibition of membrane binding (note the near-complete cytosolic distribution in WT $\text{G}\gamma 9$ - black filled circle in Fig. 3D), while $\text{G}\gamma 3_{\text{G}\gamma 9\text{PC}}$ showed a near-complete inhibition of membrane anchorage (compare the partial cytosolic distribution in WT $\text{G}\gamma 3$ - Red open circle in Fig. 3D) (Fig. 3C, 3D and Table 3- $\text{G}\gamma 9_{\text{G}\gamma 3\text{PC}}$ and $\text{G}\gamma 3_{\text{G}\gamma 9\text{PC}}$). Though the images here represent the most abundant phenotype, the grouped box chart shows the percent abundance of each phenotype of the respective $\text{G}\gamma$ mutant (Fig. 3C and 3D). Interestingly, compared to $\text{G}\gamma 9$ -WT, $\text{G}\gamma 9_{\text{G}\gamma 3\text{PC}}$ also shows a significant reduction in the near-complete inhibition phenotype (from ~100% in WT to ~24% in the mutant) (Fig. 3C, 3D and Table 3- $\text{G}\gamma 9_{\text{G}\gamma 3\text{PC}}$, black). This phenotype additionally showed a significantly faster mobility compared to that of the partial cytosolic phenotype (complete cytosolic: 5 ± 3 s, partial cytosolic: 55 ± 11 s, one-way ANOVA: $F_{1,36} = 477.158, p = 0.0001$) (Fig. 3E and Table 2- $\text{G}\gamma 9_{\text{G}\gamma 3\text{PC}}$), which is the most abundant phenotype (~75%) of Fluvastatin-exposed cells (Fig. 3D - $\text{G}\gamma 9_{\text{G}\gamma 3\text{PC}}$, red). However, Fluvastatin exposed $\text{G}\gamma 3_{\text{G}\gamma 9\text{PC}}$ cells only exhibited near-complete cytosolic phenotype (from 0% in WT to ~99% in the mutant) (Fig. 3D and Table 3- $\text{G}\gamma 3_{\text{G}\gamma 9\text{PC}}$, black), eliminating the partial cytosolic phenotype (Fig. 3D and Table 3- $\text{G}\gamma 3_{\text{G}\gamma 9\text{PC}}$, red). Mobility data confirmed the complete inhibition of membrane association (Fig 3E and Table 2- $\text{G}\gamma 3_{\text{G}\gamma 9\text{PC}}$). This is distinctly different from the response of WT $\text{G}\gamma 3$ cells to Fluvastatin treatment (Fig. 2B, Fig. 3D- Red open circle). Further, by exposing these pre-CaaX mutants to prenyltransferase inhibitors, we show that pre-CaaX switching did not change their type of prenylation (Fig. 3C-FTI and GGTI-bottom two panels). For instance, similar to $\text{G}\gamma 9$ -WT, the $\text{G}\gamma 9_{\text{G}\gamma 3\text{PC}}$ mutant showed sensitivity to FTI but not to GGTI. We have confirmed this phenotype data by examining their mobility $t_{1/2}$ (Fig. 3E and Table 2- $\text{G}\gamma 9_{\text{G}\gamma 3\text{PC}}$ and $\text{G}\gamma 3_{\text{G}\gamma 9\text{PC}}$).

3.4 Hydrophobicity character of near prenyl-Cys residues indicates statin sensitivity of G γ

Next, we focused on the pre-CaaX region hydrophobicity in determining the statin sensitivity of G γ . We employed a G γ 3 mutant, in which the *Phe-duo* adjacent to prenyl-Cys is replaced with two *Gly* residues (G γ 3_{FF \rightarrow GG}: NPFREKK**GG**CALL), and a G γ 9 mutant carrying two *Phe* residues in place of *Gly* (G γ 9_{GG \rightarrow FF}: NPFKEK-**FF**CLIS) (41). Unlike in G γ 9-WT, which showed ~100% near-complete cytosolic phenotype, the G γ 9_{GG \rightarrow FF} mutant showed a significant reduction in membrane anchorage inhibition down to ~69% while its partial inhibition cytosolic population increased to ~31% (Fig. 4B, C and Table 3- G γ 9_{GG \rightarrow FF}). These full and partial phenotypes were further confirmed using mobility rates (Fig. 4D and Table 2- G γ 9_{GG \rightarrow FF}). However, the anchorage inhibitory effect upon FTI, but not due to GGTI, showed that the prenylation type of this G γ 9_{GG \rightarrow FF} mutant remained unchanged (farnesylated). Similarly, compared to G γ 3-WT, however, more substantially, the Fluvastatin exposed G γ 3_{FF \rightarrow GG} mutant cells exhibited a higher susceptibility to membrane anchorage inhibition, in which the near-complete cytosolic distribution became the prominent phenotype (~83%) (Fig. 4B, C and Table 3- G γ 3_{FF \rightarrow GG}, black and 4D and Table 2-G γ 3_{FF \rightarrow GG}), while the partial inhibition was reduced (~17%) (Fig. 4B-D and Table 3- G γ 3_{FF \rightarrow GG}, red). The sensitivity to GGITs and lack thereof to FTIs indicated that the type of prenylation of this G γ 3_{FF \rightarrow GG} mutant remained unchanged (geranylgeranylated) (Fig. 4B and D- G γ 3_{FF \rightarrow GG}). Building on these observations, we propose that G γ 9_{GG \rightarrow FF} is a gain-of-function mutant in which the gain is the resistance to statin sensitivity. However, the gain here is smaller than the significant loss observed in G γ 3_{FF \rightarrow GG} that we identified as the loss of function mutant. We then examined the individual contribution of each *Phe* residue in the *Phe-duo* towards prenylation efficacy. We generated two G γ 3 mutants, G γ 3_{F70G} and G γ 3_{F71G}, and examined their statin sensitivity (Fig. S1). Based on their sensitivity to GGTI, we confirmed that both mutants are geranylgeranylation sensitive (Fig. S1). Compared to G γ 3-WT (Fig. 1B and 1C), a significantly higher fraction of both mutant cell populations showed near-complete inhibition of membrane localization (G γ 3_{F70G}: ~29%, G γ 3_{F71G}: ~20%) (Fig. S1 and Table 3-G γ 3_{F70G} and G γ 3_{F71G}-black). Considering that the near-complete inhibition is absent in G γ 3-WT, these data indicate a crucial role of each *Phe* for G γ 3 to gain its efficient prenylation. Further, compared to the 55 \pm 13 s mobility $t_{1/2}$ observed in Fluvastatin exposed G γ 3-WT, both the mutants showed enhanced mobility (G γ 3_{F70G}: 38 \pm 6 s, G γ 3_{F71G}: 40 \pm 8 s) in their partial inhibition populations (Table 2). This suggests that the extent of statin sensitivity in the partially inhibited population is much greater in the absence of each residue of the *Phe-duo*. These data collectively demonstrate that the hydrophobic character of the residues adjacent to prenyl-Cys is a crucial determinant of G proteins' statin sensitivity.

To further confirm the influence of prenyl-Cys adjacent hydrophobic residues on the protein's statin sensitivity, we altered the G γ pre-CaaX hydrophobicity by mutating the *Phe-duo* in G γ 3. When the *Phe-duo* is mutated to two *Leu* residues, which has a similar hydrophobicity as *Phe* (44, 45), similar to the wild-type (G γ 3 WT), the majority of the G γ 3_{FF \rightarrow LL} (NPFREKK**LL**CALL) mutant cells still showed partial inhibition of membrane anchorage (~96%) primarily (Fig. 4B, C and Table 3- G γ 3_{FF \rightarrow LL}, red), while a minor percentage (~4%) showed a near-complete inhibition (Fig. 4C and Table 3- G γ 3_{FF \rightarrow LL}, black). Interestingly mutants generated by replacing the *Phe-duo* either with *Val*, *Ala*, or *Tyr* (G γ 3_{FF \rightarrow VV}, G γ 3_{FF \rightarrow AA}, or

G γ 3_{FF \rightarrow YY}), which possess significantly lower hydrophobicity indices than *Phe* (44, 45), showed a prominent (~95-100%) near-complete membrane localization inhibition upon Fluvastatin exposure (Fig. 4B, C and Table 3). To obtain quantitative data corroborating the imaging observations, we next examined mobilities of mutant G γ subunits under pharmacological perturbation. While the mobility of partially inhibited G γ 3_{FF \rightarrow LL} was similar to that of G γ 3-WT (Fig. 1C-G γ 3 WT), completely inhibited populations of the rest of the mutants containing less hydrophobic residues adjacent to their prenyl-Cys (G γ 3_{FF \rightarrow VV}, G γ 3_{FF \rightarrow YY}, G γ 3_{FF \rightarrow AA}) exhibited significantly faster mobility upon Fluvastatin treatment (Fig. 4D and Table 2). The similar and substantially slower mobility of Fluvastatin-treated G γ 3-WT and G γ 3_{FF \rightarrow LL} indicates the considerable presence of a prenylated G γ population bound to membranes, suggesting their significant resistance to membrane localization inhibition by statins. Contrastingly, significantly faster mobility of G γ 3_{FF \rightarrow VV}, G γ 3_{FF \rightarrow YY}, and G γ 3_{FF \rightarrow AA} (Fig. 4D and Table 2) were also closer to the mobility of cytosolic G γ 9-WT observed in Fluvastatin-treated cells (Fig. 1C- G γ 9 WT), indicating that even for G proteins undergoing geranylgeranylation, the hydrophobic character of the pre-CaaX is a crucial regulator of their prenylation process. We also observed that the above G γ 3 mutations did not alter the prenylation type (Fig. 4B, D and Table 2, FTI and GGTI).

Interestingly, our data show that GGTI-mediated geranylgeranylation inhibition is partial in highly hydrophobic pre-CaaX residues carrying G γ 3 WT and G γ 3_{FF \rightarrow LL} mutant cells. On the contrary, GGTI induced a highly effective near-complete inhibition of geranylgeranylation in G γ 3_{FF \rightarrow VV}, G γ 3_{FF \rightarrow AA}, or G γ 3_{FF \rightarrow YY} mutants (Fig. 4B and D). Here, we hypothesize that compared to the above three mutants, the observed partial prenylation in GGTI-exposed G γ 3-WT and G γ 3_{FF \rightarrow LL} mutant cells results from the enhanced hydrophobicity of their pre-CaaX region. This may allow these G γ s to undergo geranylgeranylation to a significant extent, likely using the residual geranylgeranyl transferase activity remaining in the cell. Further supporting the significance of pre-CaaX residues in regulating the prenylation process, mutant cells exposed to GGTI also showed mobility half times similar to the values observed in cells exposed to Fluvastatin (Fig. 4D and Table 2). Therefore, these data suggest that the hydrophobicity of the pre-CaaX region is a primary regulator of a G protein's resistivity to prenyltransferase inhibitors.

3.5 Optogenetically-controlled reversible unmasking-masking confirms the significance of *Ct* hydrophobic residues on prenylation and the membrane affinity of the prenylated protein

To examine how the prenylated-Cys-adjacent hydrophobic residues first influence prenylation and then regulate membrane binding of the prenylated protein, we engineered an improved light-induced dimer (iLID) system-based, blue-light-gated, monomeric photo-switch to expose and mask the *Phe-duo* of a protein with a geranylgeranylating CALL at the *Ct* (iLID_{FCALL}). Since iLID is ending with a *Phe* (F449), the *Ct* sequence of the protein is —FFCALL (46) (Fig. 5A-top and B). Upon prenylation, this protein should become iLID_F with ending geranylgeranylated and carboxymethylated Cys. With the incorporated second *Phe* (F550), we created a *Phe-duo* (Fig. 5A-top) in the protein Venus-iLID_{FCALL} (Fig. 5B). Upon blue light exposure, both before and after prenylation, we expected the *Phe-duo* of the protein to be exposed (Fig. 5B).

When Venus-iLID_{FCALL} was expressed in HeLa cells, it showed primarily a cytosolic distribution with a minor Golgi localization (Fig. 5C-top, No BL). To quantify the subcellular distribution of this protein, we calculated the normalized Venus fluorescence ratio of the Golgi and nucleus. Since the prenylation-lacking Venus-iLID_{FCALL} showed a uniform cytosolic and

nuclear distribution, the fluorescence ratio was ~ 1 . The minor Golgi distribution was signified by the Golgi: Nucleus fluorescence ratio of 1.3 ± 0.1 (Fig. 5C-top box plot) before blue light (Fig. 5C-top box plot). It has been demonstrated that prenylation of CaaX sequence at the C-terminus of a protein alone is insufficient for proteins to interact with the plasma membrane (47-50). Therefore, it was unclear whether the observed primarily cytosolic localization of the protein is due to the masked *Phe-duo* in the J α helical conformation of the prenylated protein or limited prenylation of the protein polypeptide, again due to the masked *Phe-duo* (39). When we exposed cells to blue light (445 nm) to activate the photoswitch while imaging Venus at 515 nm excitation and 542 ± 30 nm emission at 1 Hz frequency, a robust and Golgi-exclusive Venus recruitment was observed upon with a $t_{1/2} = 2 \pm 1$ s, which is also signified by the significantly increased Golgi: Nucleus fluorescence ratio (1.7 ± 0.2) (one-way ANOVA: $F_{1,23} = 44.393$, $p < 0.001$) (Fig. 5C-Top, 5D-plot, and Movie S1). The Golgi recruitment of Venus accompanied a complementary reduction of cytosolic Venus fluorescence. The recruitment to the Golgi was confirmed using the co-localization of Venus with the trans-Golgi marker, GalT-dsRed (Fig. 5F and Movie S2). We further confirmed that this recruitment is Golgi targeted, by showing that the ER marker CFP-KDEL does not overlap with the Venus recruited regions upon blue light exposure (Fig. 5F). After the Venus fluorescence in Golgi reaches the steady state, termination of blue light resulted in dislodging of Golgi-bound iLID to near pre-blue light level (Fig. 5C- Top images, 5D, and Movie S1). Keeping the cells in the dark for ~ 5 minutes allowed the complete reversal of Venus fluorescence to the cytosol (Movie S1). These observations suggested that a fraction of the prenylated protein remains cytosolic before blue light exposure. Unmasking the *Phe-duo* promotes its interaction with the Golgi membrane. Blue light termination associated *Phe-duo* masking disrupts this interaction. These observations validate our hypothesis that the prenyl anchor adjoining *Phe-duo* is crucial in promoting protein-membrane interactions. Next, to examine whether the masked *Phe-duo* in Venus-iLID_{FCALL} determines its prenylation potential during protein expression, we exposed cells to 450 nm blue LED light (5-second ON-OFF cycles for 12 hours in a CO₂ incubator). The resultant cells showed a significant Golgi localization of Venus with Golgi: Nucleus of 1.6 ± 0.1 , which increased to 1.8 ± 0.1 , upon blue light exposure (one-way ANOVA: $F_{1,18} = 4.893$, $p = 0.040$) (Fig. 5C-middle). As a control experiment, we generated a Venus-iLID variant with an exposed *Phe-duo* by placing a linker sequence (GGGG) between iLID and *Phe-duo* (FF) (Venus-iLID_{GGGGFFCALL}) (Fig. 5C-bottom). Compared to the cytosolic distribution observed upon expression of Venus-iLID_{FCALL}, Venus-iLID_{GGGGFFCALL}, showed an enhanced Golgi and a detectable ER distribution (Fig. 5C-bottom). The Golgi: Nucleus Venus ratio (1.8 ± 0.2) was the highest here, with very low Venus fluorescence in the nucleus. This is expected since in Venus-iLID_{GGGGFFCALL} expressing cells, prenyl-Cys-adjacent *Phe-duo* is exposed and free to interact with endomembrane. It was also not surprising that the blue light irradiation did not significantly change the distribution in Venus (Golgi: Nucleus 1.9 ± 0.1) (one-way ANOVA: $F_{1,22} = 1.759$, $p = 0.198$) (Fig. 5C-bottom). These data indicated that, in addition to the prenyl group, membrane-accessible hydrophobic residues significantly enhance the membrane interaction of the engineered protein. Further, the decreasing presence of nuclear fluorescence from Fig. 5C top to bottom panels suggested that prenylated proteins do not enter the nucleus.

When cells are exposed to 10 μ M GGTI286 during protein expression, Venus in both Venus-iLID_{FCALL} and Venus-iLID_{GGGGFFCALL} showed completely cytosolic distributions indicating these proteins are geranylgeranylation sensitive (Fig. 5E). Furthermore, the blue light irradiation did not recruit Venus to the Golgi in Venus-iLID_{FCALL} under GGTI286 treated

conditions (Fig. 5E). To further confirm that geranylgeranylation is required for Golgi recruitment of this protein, we examined Venus-iLID_{FCALL} expressing cells under FTI, GGTI, or Fluvastatin-treated conditions. Both Fluvastatin-treated and GGTI-treated cells showed uniform Venus distribution throughout the cytosol and the nucleus, and failed to show blue light-induced Venus recruitment to Golgi (Fig. 5E top and S3-A). However, cells upon FTI treatment (only inhibits farnesylation) behaved similarly to control cells and exhibited blue light-induced Venus recruitment to Golgi (Fig. S3-A). To emphasize that blue light-induced Golgi recruitment of these two proteins depends on their prenylation state, we used C→A mutant versions of iLID_{FCALL} and iLID_{GGGGFFCALL} (Venus-iLID_{FAALL} and Venus-iLID_{GGGGFFAALL}) that showed complete cytosolic distribution before blue light exposure and no sensitivity to blue light irradiation (Fig. S3-B).

Overall, the data suggest that overnight blue light exposure during protein expression enhances the prenylation since the *Phe-duo* in the photoswitch is continuously exposed, improving polypeptide-membrane interactions. The significant nuclear localization of Venus in Venus-iLID_{FCALL} cells (due to reduced prenylation) and the reduced presence of nuclear-Venus in Venus-iLID_{GGGGFFCALL} cells and overnight blue light exposed Venus-iLID_{FCALL} cells (due to enhanced prenylation) also collectively suggest that the unmasked *Phe-duo* enhances the prenylation efficacy. For instance, Venus-iLID_{FCALL} cells exposed to overnight blue light must have enhanced prenylation efficacy and thus a significantly higher concentration of Venus – iLID_{FC} ^{-OMe} _{-gerger} proteins compared to the control cells, as reflected by the significantly elevated Golgi localization of Venus. Collectively, these experiments demonstrate a previously unknown mechanism of polypeptide prenylation regulation. To our knowledge, this is the first presentation for dynamic control of molecular interactions using reversible optogenetics to regulate membrane interactions of lipidated proteins.

3.6 Contribution of pre-CaaX positively charged residues on G γ prenylation efficacy and statin sensitivity is moderate, however significant

Both G γ 3-WT and G γ 9-WT contain homologous sequences consisting of positively charged *Lys*, *Arg* residues, or both at the beginning of their pre-CaaX regions (Fig. 3A). Our previous work indicated that the positively charged side chains of these residues help G γ to maintain transient interactions with the phospholipid head groups of the membrane (41). To understand the collective role of hydrophobic and positively charged residues on enhanced membrane interactions of G γ 3-WT, we systematically mutated the pre-CaaX of G γ 9 to gradually achieve G γ 3-like characteristics without changing the prenylation type. Even though both *Lys* and *Arg* are positively charged, to examine whether G γ 3 achieved its improved membrane interactions and thereby resistance to Fluvastatin-induced inhibition of its membrane anchoring due to the higher geometric stability provided by *Arg* (51), we mutated the 61st *Lys* in G γ 9 to *Arg* (G γ 9_{KEK-GG \rightarrow REK-GG}). It has been reported that compared to *Lys*, the guanidinium group of *Arg* allows the formation of stable and a larger number of electrostatic interactions in three different directions (51). The higher pKa of *Arg* may also contribute to forming more stable ionic interactions than *Lys* (51). Only ~84% of the G γ 9_{KEK-GG \rightarrow REK-GG} mutant cells exhibited near-complete cytosolic distribution compared to ~100% in G γ 9-WT (Fig. 6A, 6B and Table 3-G γ 9_{KEK-GG \rightarrow REK-GG}). The appearance of a ~16% cell population with partial cytosolic phenotype is also indicated by 45±9 s mobility t_{1/2}, as opposed to the 9±5 s t_{1/2} of G γ 9 (Fig. 6C and Table 2-G γ 9_{KEK-GG \rightarrow REK-GG}). These data showed that the pre-CaaX *Arg* grants G γ 3 a higher membrane

affinity, thereby increasing prenylation efficacy and reducing statin sensitivity. Next, to understand the role of the additional *Lys* residue at the 69th position of $\text{G}\gamma 3\text{-WT}$, we introduced an additional *Lys* to this mutant, creating the $\text{G}\gamma 9_{\text{KEK-GG}\rightarrow\text{REKKGG}}$ mutant. Compared to both the wild type and $\text{G}\gamma 9_{\text{KEK-GG}\rightarrow\text{REK-GG}}$ cells expressing $\text{G}\gamma 9_{\text{KEK-GG}\rightarrow\text{REKKGG}}$ showed further reduced sensitivity to Fluvastatin (~65% near-complete membrane anchorage inhibition) (Fig. 6A, 6B and Table 3- $\text{G}\gamma 9_{\text{KEK-GG}\rightarrow\text{REKKGG}}$). This mutant also showed increased partial inhibition (~36% cell) (Fig. 6B and Table 3- $\text{G}\gamma 9_{\text{KEK-GG}\rightarrow\text{REKKGG}}$). These data indicate that basic pre-CaaX residues significantly enhance the prenylation efficacy while reducing the statin sensitivity of $\text{G}\gamma 3$. Building on this, we next generated a $\text{G}\gamma 9$ mutant ($\text{G}\gamma 9_{\text{KEK-GG}\rightarrow\text{KEKKFF}}$) to understand the cumulative effect of the additional *Lys*69 and the *Phe-duo* in $\text{G}\gamma 3$ pre-CaaX. Compared to $\text{G}\gamma 9\text{-WT}$, $\text{G}\gamma 9_{\text{KEK-GG}\rightarrow\text{KEKKFF}}$ mutant cells exhibited elevated prenylation efficacy and reduced statin sensitivity, indicated by the significantly reduced near-complete membrane anchorage inhibition to ~51%, and the increased partial inhibition to ~48% (Fig. 6A, 6B and Table 3). This mutant only differs from the $\text{G}\gamma 9_{\text{KEKGG}\rightarrow\text{KEKKFF}}$ mutant by having an additional *Lys*, which increases the partial inhibition from ~16% to ~51%. The sensitivity of these mutants to FTI, but not to GGTI, confirmed that their prenylation type is unchanged and remains farnesylated.

4. Discussion

Post-translational modifications play central roles in membrane association of the G proteins such as Ras superfamily G proteins and heterotrimeric G proteins (33). Since G protein signaling pathways mediate a vast array of physiological responses, their dysregulation contributes to many diseases, including cancer, heart disease, hypertension, endocrine disorders, and blindness (52). In an early study, we showed that $\text{G}\gamma$ membrane interactions and associated signaling are inhibited in the presence of statins, likely due to the inhibition of prenylation. However, in the same study, we also observed differential extents of membrane interaction inhibition among different $\text{G}\gamma$ subtypes (13). In the present study, we attempted to identify the molecular reasoning for this differential inhibition.

Though prenylation is essential, it alone is insufficient for the plasma membrane interaction of prenylated G proteins (47-50). Studies show that in addition to the prenyl anchor, the amino acids antecedent to the CaaX motif further support membrane anchorage of proteins (40-42, 48, 49, 53, 54). However, in the absence of prenylation, the contributions of membrane-interacting Ct residues alone are not sufficient to support the recruitment of a protein to a membrane (13, 38). The positively charged poly *Lys* region on KRas-4b is a classic example showing the participation of prenyl-*Cys*-adjacent amino acids in targeting prenylated proteins to the plasma membranes (48, 49, 53). Here, KRas-4b □ membrane interaction is maintained by the thermodynamically favored insertion of the farnesyl lipid anchor into the membrane lipid bilayer, in concert with the electrostatic interactions of the 10 *Lys* residues (positively-charged) in the pre-CaaX region with the negatively charged polar headgroups of the plasma membrane phospholipids (53). It has also been shown that the polybasic residues in the pre-CaaX region of a protein can function as a sorting signal to prevent proteins from entering the Golgi (55). HRas is another example of containing a *Cys* residue adjacent to CaaX as a second signal to which a palmitoyl anchor is attached. The palmitoyl anchor on HRas serves as a second signal to traffic the protein to different targeted cell membranes (55). Along with the above evidence from previous literature, we have recently established that the *Phe-duo* adjacent to prenylated *Cys* in some $\text{G}\gamma$ subunits significantly promotes stronger membrane anchorage of $\text{G}\gamma$ (41). Two

prenylation types and variable second signals encoded by the pre-CaaX region have been suggested to target a protein to different microdomains within the plasma membrane (55).

Even though the twelve G γ types are prenylated with either one of the two prenyl anchors; 15-C farnesyl or 20-C geranylgeranyl, they exhibit a broad range of membrane affinities, spanning from the lowest membrane affinity observed in farnesylated G γ 9 to the highest in geranylgeranylated G γ 3 (40-42). When G γ s are prenylated, they reside at the inner leaflet of the plasma membrane as G $\alpha_{\text{GDP}}\beta\gamma$ heterotrimer, bound to or near GPCRs (56, 57). When GPCRs are activated, G α exchanges the bound GDP to GTP, dissociating the heterotrimer into G α_{GTP} and G $\beta\gamma$. Upon GPCR activation, all G γ members support G $\beta\gamma$ translocation from the plasma membrane to the endomembrane in a G γ type-specific manner (40, 54). These G γ type-dependent translocation rates and extents have been used as a measure of the membrane affinity of a specific G γ (40-42, 54, 58-60). According to this classification, the three G γ s with the highest membrane affinities (G γ 2, γ 3, and γ 4) contain two conserved *Phe* residues that we named the *Phe-duo*, next to the prenylated and carboxymethylated *Cys* (41). An early study suggested that aromatic residues such as *Phe* in the membrane-interacting domain of a protein enhance membrane-protein interactions via a hydrophobic binding (61). This enhanced interaction is achieved by inserting the hydrophobic side chains into the fatty acid tail region of the lipid bilayer (61). Our recent work also indicated that the aromatic side chain of *Phe* residues is crucial for the enhanced membrane affinity of G γ 2, 3, and 4 (41). In contrast, the G γ with the lowest membrane affinity, G γ 9, possesses two less hydrophobic *Gly* residues at the corresponding position. This lowest membrane affinity can easily be understood by considering G γ 9 prenylation type (farnesylation) and its less hydrophobic pre-CaaX region.

When the statin sensitivities of the 12 G γ subtypes were examined by measuring the inhibition of membrane anchoring, we observed a partial perturbation of membrane anchorage in G γ 2, 3, 4, 7, 8, and 12. Interestingly, the same G γ subtypes also exhibited a partial sensitivity to the GGTI. We propose the highly effective prenylation efficacy of G γ 2, 3, 4, 7, 8, and 12 allows them to achieve some prenylation by utilizing the residual geranylgeranyl transferase activity remaining under GGTI. These results also indicated that using the CaaX motif sequence to determine the type of prenylation is correct, and mobility $t_{1/2}$ is a reliable measure of the G protein prenylation efficacy (62, 63). However, the complete to partial Fluvastatin sensitivity of geranylgeranylation-sensitive G γ s raised the question of whether this membrane anchorage inhibitions depends on the type of prenylation at all. To answer this question, we systematically mutated the CaaX and pre-CaaX regions of G γ 3 and G γ 9 since these two G γ s exhibited two extremities of Fluvastatin sensitivity out of 12 G γ subtypes. The results from G γ 9_{CALL} and G γ 3_{CHIS} ruled out our hypothesis that G γ sensitivity to statin is determined by the type of prenylation since both G γ 9_{CALL} and G γ 3_{CHIS} mutants retained their wildtype's statin sensitivity despite the switched prenylation type. The significant change in statin sensitivity observed in G γ 9_{G γ 3PC} and G γ 3_{G γ 9PC} mutants further confirmed that G γ 's sensitivity to statins is independent of prenylation type while highlighting a major role of pre-CaaX region in this process. Focusing on our early finding that *Phe-duo* in pre-CaaX regions adjacent to prenylated *Cys* plays a major role in membrane interactions of high membrane affinity G γ s, using G γ 9_{GG \rightarrow FF} and G γ 3_{FF \rightarrow GG} mutants, we next examined the influence of the *Phe-duo* on G γ prenylation efficacy under statin-treated conditions. Our observations suggested that the hydrophobic residues in the pre-CaaX region control the prenylation efficacy of G γ .

Our optogenetic approach that allowed reversible unmasking-masking of *Phe-duo* further emphasized the importance of *Phe-duo* on protein prenylation and membrane interaction of

prenylated proteins. When the pre-CaaX FF is masked, we propose that the protein has a low prenylation efficacy. Indicating the multi-level regulation imposed, only a small fraction of the prenylated population binds Golgi before blue light, and pre-CaaX unmasking is required for its membrane binding. Although the exact reason is unclear, it has been shown that when other proteins do not support them, prenylated G proteins accumulate primarily at the Golgi, not in ER or the plasma membrane (64). Optical activation-induced Golgi recruitment of iLID model protein agrees with this. When the prenylated protein population is increased, we propose that the excess proteins Golgi cannot accommodate interact with the ER. This is evident from the major Golgi and minor ER distribution of the iLID model protein in cells exposed to blue light pulses overnight. In the iLID protein with GGGGFF pre-CaaX motif, the FF is constitutively unmasked, increasing prenylation. This protein shows both Golgi and ER localization.

Our observations upon altering positively charged residues of $G\gamma$ pre-CaaX, in which *Lys* and *Arg* influenced, however, differently, both the statin as well as the prenyl transferase inhibitor sensitivity is consistent with the expected contribution of basic residues on membrane interaction of a protein (65-67). Considering the positively charged pre-CaaX of $G\gamma^9_{G\gamma 3PC}$ due to the presence of an *Arg* and an extra *Lys* in the pre-CaaX promoting membrane interactions, the similar G protein distributions observed for Fluvastatin-exposed $G\gamma^9_{G\gamma 3PC}$ (despite its farnesylation) and $G\gamma 3$ -WT can be understood. In summary, these data suggest that collectively both hydrophobic and positively charged residues in the pre-CaaX are crucial determinants of the statin sensitivity of a protein. Since prenylation takes place at the ER membrane, we also hypothesize that these pre-CaaX residues control the $G\gamma$ prenylation efficacy by contributing to $G\gamma$ polypeptide interactions with endomembrane and/or prenyltransferases during prenylation, post-prenylation processing, or both through their transient membrane interactions.

When the overall data summary is considered, it also appears that the contribution to the gain or loss of prenylation efficacy by a pre-CaaX residue is dependent on the type, number, location of other residues (composition of the pre-CaaX). When considering the relative roles of pre-CaaX and prenylation (and carboxymethylation), our data clearly shows that the latter is the major membrane recruiter, however, the efficacy of prenylation is pre-CaaX dependent, specially under suboptimal conditions. Regardless of their highly hydrophobic and/or positively charged pre-CaaX regions C→A versions of these $G\gamma$ mutants exhibited completely cytosolic distributions and faster mobilities (Fig. S2), because pre-CaaX alone, without the prenyl anchor, cannot support membrane binding of a protein. To rule out bias in imaging data analysis, in addition to quantification of $G\gamma$ mobility with different treatment conditions, we carried out a blind control experiment with an experimenter who is blind to the type of mutation and the treatment condition. When compared, the results obtained by the blind control experimenter and the experimenter using one-way ANOVA, we did not observe a significant difference (Fig. S4). We further support our data by providing multi-cell images representing different phenotypes of each population of $G\gamma$, WTs or their mutants in response to different treatments (Fig. S5 and 6).

In our previous study, we conclusively demonstrate that statins can differentially perturb $G\beta\gamma$ signaling in a $G\gamma$ type-specific manner by potentially inhibiting $G\beta\gamma$ -membrane interactions (13). The data from the current study provides a clear molecular explanation for this previously observed differential statin sensitivities, by revealing the collective role of hydrophobic and positively charged residues in the $G\gamma$ pre-CaaX region play. Given the cell and tissue-specific distribution of 12 $G\gamma$ types with distinct pre-CaaX motifs in the body, our data may provide a molecular justification for diverse pleiotropic effects of statins due to $G\gamma$ -dependent perturbation of $G\beta\gamma$ signaling (68-71). Additionally, our data also suggest that the extent of a G protein's

sensitivity to prenyltransferase inhibitors is also influenced by the nature of its pre-CaaX region. Due to the involvement of Ras family G proteins and some G γ subtypes in oncogenesis (72-75), prenyltransferase inhibitors have been explored for chemotherapy (76). Tipifarnib, Lonafarnib, BMS-214662, L-778, and L-123 are a few farnesyltransferase inhibitors tested in phase-II clinical trials. Nevertheless, they failed, and the mutations acquired in the oncogene or cancer reaching the metastatic state were considered culprits (15, 77). We propose that examining the pre-CaaX composition of the oncogenic G proteins in specific tumors may allow revisiting these inhibitors for treating certain cancers.

Conclusion

Switching the intact prenylation and statin sensitivity observed upon switching the CaaX motif between G γ 3 and G γ 9 indicated that the CaaX residues of the unprenylated polypeptide do not have a significant role governing protein-membrane interaction, as well as the prenylation efficacy. The perturbations we made in the pre-CaaX of G γ indicate that residues provide varying, and specific contributions to either gain or loss of statin, as well as prenyl transferase inhibitor sensitivities depending on the properties, location, and the number on the pre-CaaX. For instance, the *Phe-duo* in G γ 9 pre-CaaX environment only has a lesser contribution from gaining the sensitivity compared to their role in G γ 3 pre-CaaX environment. Overall, the results indicate that despite the prenylation type, the molecular properties of the G γ pre-CaaX region regulate their prenylation efficacy. When the prenylation process is suboptimal, either because of limited prenyl lipid substrate availability due to pharmacological (statins) or genetic constraints or limited prenyltransferase activity (due to prenyltransferase inhibitors), or both, our data clearly show that different G γ types, depending on their pre-CaaX show distinct prenylation responses. This allows G protein-GPCR signaling in cells and tissues with particular G γ types to be differentially regulated by statins and prenyltransferase inhibitors. Considering the involvement of G proteins in physiology and pathology, the discovered molecular interactions that govern the prenylation process may help design more efficient and cellular-genetic-make-up-dependent regulators for G protein signaling. All the prenyltransferase inhibitors have advanced only up to phase II clinical trials as cancer therapeutics. Additionally, our results also shed light on potential future combinatorial statin-transferase inhibitor therapies for a variety of diseases, including cancer.

2. Materials and methods

2.1 Reagents

The reagents used were as follows; Fluvastatin, Tipifarnib, and GGTI286 (Cayman Chemical, Ann Arbor, MI) were dissolved in appropriate solvents according to the manufacturer's instructions and diluted in 1% Hanks' Balanced Salt solution (HBSS) supplemented with NaHCO₃ or regular cell culture medium before being added to cells.

2.2 DNA constructs and cell lines

For the engineering of DNA constructs used, GFP-G γ 9_{G γ 3PC}, GFP-G γ 9_{GG \rightarrow FF}, G γ 3_{FF \rightarrow GG}, mCh-G γ 3_{C72A} YFP-tagged G γ 1–G γ 13, GFP-G γ 9, GFP-G γ 3, GFP-G γ 9_{CALL}, GFP-G γ 3_{CIIS}, CFP-KDEL, and GalT-dsRed have been described previously (13, 41, 54, 78). Dr. Brian Kuhlman from the University of North Carolina at Chapel Hill, North Carolina kindly provided permission to use iLID construct. G γ 3, G γ 9 mutants, and iLID constructs were generated by PCR

amplifying the parent constructs in pcDNA3.1 (GFP-G γ 3, GFP-G γ 9, and Venus-iLID) with overhangs containing expected nucleotide mutations and DpnI (NEB) digestion (to remove the parent construct) followed by Gibson assembly (NEB) (79). Cloned cDNA constructs were confirmed by sequencing (Genewiz). The HeLa cell line was originally purchased from the American Type Culture Collection (ATCC) and authenticated using a commercial kit to amplify nine unique STR loci.

2.3 Cell culture and transfections

HeLa cells were cultured in minimum essential medium (MEM-Cellgro) with 10% heat-inactivated dialyzed fetal bovine serum (DFBS; from Atlanta Biologicals) and 1% penicillin–streptomycin (PS) in 60 mm tissue culture dishes and maintained in a 37°C, 5% CO₂ incubator. When the cells reached ~80% confluency, they were lifted from the dish using versene-EDTA (Cell-Gro) and resuspended in their growth medium at a cell density of 1×10^6 /ml. For imaging experiments (G γ subcellular distribution analysis, fluorescence recovery after half-cell photobleaching for G γ mobility analysis, subcellular distribution analysis, and blue light-induced membrane interaction analysis of Ct-modified iLID), cells were seeded on 35 mm cell culture–grade glass-bottomed dishes (Cellvis) at a density of 8×10^4 cells. The day following cell seeding, cells were transfected with appropriate DNA combinations (YFP-tagged G γ 1–G γ 13: 0.8 μ g, GFP tagged G γ or G γ mutants: 0.2 μ g, Venus-iLID_{FCALL} and Venus-iLID_{GGGGFFCALL}: 0.8 μ g per each dish) using Lipofectamine 2000 transfection reagent (Invitrogen) according to the manufacturer’s protocol and stored in a 37°C, 5% CO₂ incubator. After 3.5/5 hours of transfection, cells were replenished with the growth medium containing either dimethyl sulfoxide (DMSO) or the respective inhibitor (Fluvastatin, FTI, or GGTI). Live-cell imaging was performed ~16 hours post-transfection.

2.4 Live cell imaging, half-cell photobleaching, iLID photoactivation, image analysis, and data processing

Live-cell imaging experiments were performed using a spinning disk (Dragonfly 505) XD confocal TIRF imaging system composed of a Nikon Ti-R/B inverted microscope with a 60X, 1.4 NA oil objective and iXon ULTRA 897BVback-illuminated deep-cooled EMCCD camera. Photobleaching and photoactivation of spatio-temporally confined regions of interest (ROIs) of cells were performed using a laser combiner with 40-100 mW solid-state lasers (445, 488, 515, and 594 nm) equipped with Andor® FRAP-PA unit (fluorescence recovery after photobleaching and photoactivation), controlled by Andor iQ 3.1 software (Andor Technologies, Belfast, United Kingdom). For selective photobleaching of YFP or GFP, 488 nm (3.1 mW) and 515 nm (1.5 mW) lasers at the focal plane (60x oil 1.49 NA objective) were used. Photobleaching speed: ~100 μ s per half cell (~a 100 μ m² area). The photobleaching covers the entire depth of the cell along the Z axis. For photoactivation of iLID 445 nm laser at 6.3 μ W was used. Proteins tagged with Venus/YFP were imaged using 515 nm excitation and 542 nm emission; GFP using 488 nm excitation–515 nm emission; CFP imaging or blue light activation of optogenetically active iLID constructs were performed using 445 nm excitation and 478 nm emission. For global and confined optical activation of iLID-expressing cells, the power of 445 nm solid-state laser was adjusted to 5 mW. Additional adjustments of laser power with 0.1%-1% transmittance was achieved using Integrated Lase Engine (ILE). Data acquisition, time-lapse image analysis, processing, and statistical analysis were performed as explained previously (13).

Briefly, time-lapse images were analyzed using Andor iQ 3.1 software by acquiring the mean pixel fluorescence intensity changes of the entire cell or the selected ROIs.

2.5 Log cavity energy (Log CE) calculation γ Ct peptides (pre-CaaX+CaaX)

The hydrophobicity of a molecule can be quantified using octanol-water partition coefficient (K_{OW})-based Log Cavity energy (Log CE) value. The methodology to computationally determine Log CE using density functional theory (DFT) and the Solvent Model based on Density (SMD) was previously shown to have excellent agreement with experimental Log CE values for various molecules, including peptides (80, 81). We employed the M11 meta-functional (82) with SMD (83) and computed the Log CE using the equation, $\text{Log CE} = -\frac{(\Delta G_{\text{octanol}} - \Delta G_{\text{water}})}{2.303RT}$ for the unprenylated γ polypeptide (consisting pre-CaaX and CaaX regions) and prenylated and carboxymethylated Ct peptides representing the γ family members at 37 °C (310 K). The peptides structures were optimized with a split-valance basis (3-21G*), and the solvation energies (Table S1) were computed with a polarized triple-zeta basis set (6-311+G**). All computations were performed using Gaussian16 (Revision C.01) software (84).

2.6 Computationally modeled structure generation of the iLID-based photoswitch

We used the amino acid sequence of iLID(46) to generate the modeled protein structures in Fig. 5A and B using AlphaFold2. First, we added the respective additional amino acids 'FCALL' and 'GGGGFFCALL' at the C terminus of the iLID to generate iLID_{FCALL} and iLID_{GGGGFFCALL}. Then we fed these sequences to AlphaFold2 and built homology models. Structures that best fit the experimental iLID structure (PDB ID: 4WF0) were selected for protein folding validation. Finally, the protein preparation tool in Schrodinger Maestro13.3.121 was used to optimize the selected protein model. When generating the modeled iLID_{FCALL}^{-OMe_{gerger}} (before blue light irradiation), we used the 3D builder tool of Schrodinger and generated the carboxymethylated geranylgeranylated *cys* in 2D format. Then the structure was optimized using the protein preparation tool in Schrodinger Maestro for a low-energy 3D structure with corrected chirality. We followed a similar approach to generate the carboxymethylated geranylgeranylated Ct peptide (NYFFC_{gerger}^{-OMe}) of light-activated iLID_{FCALL}^{-OMe_{gerger}} in 2D format, however used the Schrodinger Maestro LigPrep tool for optimizing the 3D structure. We then depicted AANDE residues of iLID as an unstructured peptide that connects AsLOV2 of iLID with the above prepared NYFFC_{gerger}^{-OMe}. This structure is shown as the blue light activated protein in Fig. 5B.

2.7 Statistical data analysis

All experiments were repeated multiple times to test the reproducibility of the results. Statistical analysis and data plot generation were done using OriginPro software (OriginLab®). Results were analyzed from multiple cells and represented as mean ± SEM. The number of cells used in the analysis is given in respective figure legends. For $G\alpha\beta\gamma$ heterotrimer mobility analysis using fluorescence recovery after half-cell photobleaching, after obtaining all the baseline-subtracted data employing the Nonlinear Curve Fitting (NLFit) tool in OriginPro, $G\alpha\beta\gamma$ mobility dynamics plots were fitted to the ExpAssoc1 function under the Pharmacology category. For each fitting half time was calculated using, [half-time = $\ln(2)/K = \ln(2)*\text{Tau}$] equation where K is the rate constant and *Tau* is the time constant (*Tau* = 1/K). The mean values of half-time obtained from nonlinear curve fitting for all cells are given as mean mobility $t_{1/2}$. One-way ANOVA statistical tests were performed using OriginPro to determine the statistical

significance between two or more populations of signaling responses. Tukey's mean comparison test was performed at the $p < 0.05$ significance level for the one-way ANOVA statistical test.

2.8 Blind control experiment

For each mutant with different treatment conditions, the blind control experimenter was given multiple images from experiments conducted on different days and instructed to categorize each cell image for its $G\gamma$ distribution, whether cytosolic or partially cytosolic. The mean values for each category of the blind control were compared with the values observed by the experimenter. The compared mean values were found not significantly different between the blind control experimenter and the experimenter (one-way ANOVA).

Data availability

The datasets used and/or analyzed during the current study are available from the corresponding author upon reasonable request.

Acknowledgment

We thank the Department of Biology, Saint Louis University, for providing instrumentation and other support. Ohio Supercomputer Center for providing access to high-performance computing clusters and Gaussian software for DFT calculations. We also thank the Saint Louis University Institute for Drug and Biotherapeutic Innovation for providing computational resources and access to Schrödinger software, with funding from the Saint Louis University Research Institute. We also thank Ajith lab members Sithurandi Ubeyasinghe, Dhanushan Wijayarathna, Senuri Piyawardana, Chathuri Rajarathna, and Aditya Chandu for various experimental support, comments, and discussions.

Author Contribution

M.T. generated most of the $G\gamma$ mutants and Venus-iLID_{FCALL} construct unless otherwise mentioned. W.T. generated GFP tagged $G\gamma$ _{KEK-GG_→REK-GG}, $G\gamma$ _{9KEK-GG_→REKGG}, $G\gamma$ _{9KEK-GG_→KEKKEFE}, $G\gamma$ _{3F70G}, $G\gamma$ _{3F71G} mutants and Venus-iLID_{GGGGFFCALL} construct. M.T. performed the majority of the experiments. W.T. performed the mobility $t_{1/2}$ calculation experiment and data analysis for the $G\gamma$ _{3C72A} mutant and made Movie S1. W.T. computationally modeled structures in Fig 5A and B. M.T. analyzed the data and prepared the figures. J.L.P. computationally calculated the log CE of pre-CaaX+CaaX peptides of unprenylated $G\gamma$. M.T. and A.K. conceptualized the project and wrote the manuscript.

Conflict of Interest

The authors declare that they have no conflicts of interest concerning the contents of this article.

Funding

NIH-NIGMS: grant number R01GM140191

References

1. Ambrogelly, A., Palioura, S., and Soll, D. (2007) Natural expansion of the genetic code Nat Chem Biol **3**, 29-35

2. Gelb, M. H., Brunsveld, L., Hrycyna, C. A., Michaelis, S., Tamanoi, F., Van Voorhis, W. C. *et al.* (2006) Therapeutic intervention based on protein prenylation and associated modifications *Nat Chem Biol* **2**, 518-528
3. Palsuledesai, C. C., and Distefano, M. D. (2015) Protein prenylation: enzymes, therapeutics, and biotechnology applications *ACS Chem Biol* **10**, 51-62
4. Ashby, M. N. (1998) CaaX converting enzymes *Curr Opin Lipidol* **9**, 99-102
5. Winter-Vann, A. M., and Casey, P. J. (2005) Post-prenylation-processing enzymes as new targets in oncogenesis *Nat Rev Cancer* **5**, 405-412
6. Sytkowski, P. A., Kannel, W. B., and D'Agostino, R. B. (1990) Changes in risk factors and the decline in mortality from cardiovascular disease. The Framingham Heart Study *N Engl J Med* **322**, 1635-1641
7. Goldstein, J. L., and Brown, M. S. (1990) Regulation of the mevalonate pathway *Nature* **343**, 425-430
8. Alberts, A. W. (1988) Discovery, biochemistry and biology of lovastatin *Am J Cardiol* **62**, 10J-15J
9. Istvan, E. S., and Deisenhofer, J. (2001) Structural mechanism for statin inhibition of HMG-CoA reductase *Science* **292**, 1160-1164
10. Miziorako, H. M. (2011) Enzymes of the mevalonate pathway of isoprenoid biosynthesis *Arch Biochem Biophys* **505**, 131-143
11. Buhaescu, I., and Izzedine, H. (2007) Mevalonate pathway: a review of clinical and therapeutical implications *Clin Biochem* **40**, 575-584 [10.1016/j.clinbiochem.2007.03.016](https://doi.org/10.1016/j.clinbiochem.2007.03.016)
12. Chan, K. K. W., Oza, A. M., and Siu, L. L. (2003) The statins as anticancer agents *Clin Cancer Res* **9**, 10-19
13. Tennakoon, M., Kankanamge, D., Senarath, K., Fasih, Z., and Karunarathne, A. (2019) Statins Perturb G β γ Signaling and Cell Behavior in a G γ Subtype Dependent Manner *Mol Pharmacol* **95**, 361-375
14. Malumbres, M., and Barbacid, M. (2003) RAS oncogenes: the first 30 years *Nat Rev Cancer* **3**, 459-465
15. Marchwicka, A., Kamińska, D., Monirialamdari, M., Błażewska, K. M., and Gendaszewska-Darmach, E. (2022) Protein Prenyltransferases and Their Inhibitors: Structural and Functional Characterization *International Journal of Molecular Sciences* **23**, 5424
16. Wang, J., Yao, X., and Huang, J. (2017) New tricks for human farnesyltransferase inhibitor: cancer and beyond *Medchemcomm* **8**, 841-854
17. Sousa, S. F., Fernandes, P. A., and Ramos, M. J. (2008) Farnesyltransferase inhibitors: a detailed chemical view on an elusive biological problem *Curr Med Chem* **15**, 1478-1492
18. Barbalata, C. I., Tefas, L. R., Achim, M., Tomuta, I., and Porfire, A. S. (2020) Statins in risk-reduction and treatment of cancer *World J Clin Oncol* **11**, 573-588
19. Fatehi Hassanabad, A. (2019) Current perspectives on statins as potential anti-cancer therapeutics: clinical outcomes and underlying molecular mechanisms *Transl Lung Cancer Res* **8**, 692-699
20. Strykowska-Gora, A., Karczarek-Borowska, B., Gora, T., and Krawczak, K. (2015) Statins and cancers *Contemp Oncol (Pozn)* **19**, 167-175
21. Ding, X., Zhang, W., Li, S., and Yang, H. (2019) The role of cholesterol metabolism in cancer *Am J Cancer Res* **9**, 219-227

22. Wang, S. T., Ho, H. J., Lin, J. T., Shieh, J. J., and Wu, C. Y. (2017) Simvastatin-induced cell cycle arrest through inhibition of STAT3/SKP2 axis and activation of AMPK to promote p27 and p21 accumulation in hepatocellular carcinoma cells *Cell Death Dis* **8**
23. Jones, H. M., Fang, Z., Sun, W., Clark, L. H., Stine, J. E., Tran, A. Q. *et al.* (2017) Atorvastatin exhibits anti-tumorigenic and anti-metastatic effects in ovarian cancer in vitro *Am J Cancer Res* **7**, 2478-2490
24. Zaleska, M., Mozenska, O., and Bil, J. (2018) Statins use and cancer: an update *Future Oncol* **14**, 1497-1509
25. Kim, J., Choi, E. A., Han, Y. E., Lee, J. W., Kim, Y. S., Kim, Y. *et al.* (2020) Association between statin use and all-cause mortality in cancer survivors, based on the Korean health insurance service between 2002 and 2015 *Nutr Metab Cardiovasc Dis* **30**, 434-440
26. Licarete, E., Sesarman, A., and Banciu, M. (2015) Exploitation of pleiotropic actions of statins by using tumour-targeted delivery systems *J Microencapsul* **32**, 619-631
27. Wolfe, A. R., Debeb, B. G., Lacerda, L., Larson, R., Bambhroliya, A., Huang, X. *et al.* (2015) Simvastatin prevents triple-negative breast cancer metastasis in pre-clinical models through regulation of FOXO3a *Breast Cancer Res Treat* **154**, 495-508
28. Schointuch, M. N., Gilliam, T. P., Stine, J. E., Han, X., Zhou, C., Gehrig, P. A. *et al.* (2014) Simvastatin, an HMG-CoA reductase inhibitor, exhibits anti-metastatic and anti-tumorigenic effects in endometrial cancer *Gynecol Oncol* **134**, 346-355
29. Wang, H. L., Sun, N., Li, X., Li, K., Tian, J. G., and Li, J. M. (2016) Simvastatin suppresses cell migration and invasion, induces G0/G1 cell cycle arrest and apoptosis in osteosarcoma cells *Int J Clin Exp Pathol* **9**, 5837-5848,
30. Chou, C. W., Lin, C. H., Hsiao, T. H., Lo, C. C., Hsieh, C. Y., Huang, C. C. *et al.* (2019) Therapeutic effects of statins against lung adenocarcinoma via p53 mutant-mediated apoptosis *Sci Rep* **9**, 20403
31. Jiang, P., Mukthavaram, R., Chao, Y., Nomura, N., Bharati, I. S., Fogal, V. *et al.* (2014) In vitro and in vivo anticancer effects of mevalonate pathway modulation on human cancer cells *Br J Cancer* **111**, 1562-1571
32. Smrcka, A. V., and Fisher, I. (2019) G-protein $\beta\gamma$ subunits as multi-functional scaffolds and transducers in G-protein-coupled receptor signaling *Cell Mol Life Sci* **76**, 4447-4459
33. Marrari, Y., Crouthamel, M., Irannejad, R., and Wedegaertner, P. B. (2007) Assembly and trafficking of heterotrimeric G proteins *Biochemistry* **46**, 7665-7677
34. Saini, D. K., Chisari, M., and Gautam, N. (2009) Shuttling and translocation of heterotrimeric G proteins and Ras *Trends Pharmacol Sci* **30**, 278-286
35. Chisari, M., Saini, D. K., Kalyanaraman, V., and Gautam, N. (2007) Shuttling of G protein subunits between the plasma membrane and intracellular membranes *J Biol Chem* **282**, 24092-24098
36. DiGiacomo, V., Marivin, A., and Garcia-Marcos, M. (2018) When Heterotrimeric G Proteins Are Not Activated by G Protein-Coupled Receptors: Structural Insights and Evolutionary Conservation *Biochemistry* **57**, 255-257
37. Plouffe, B., Thomsen, A. R. B., and Irannejad, R. (2020) Emerging Role of Compartmentalized G Protein-Coupled Receptor Signaling in the Cardiovascular Field *ACS Pharmacol Transl Sci* **3**, 221-236
38. Mulligan, T., Blaser, H., Raz, E., and Farber, S. A. (2010) Prenylation-deficient G protein γ subunits disrupt GPCR signaling in the zebrafish *Cell Signal* **22**, 221-233

39. Kalman, V. K., Erdman, R. A., Maltese, W. A., and Robishaw, J. D. (1995) Regions outside of the CAAX motif influence the specificity of prenylation of G protein γ subunits *J Biol Chem* **270**, 14835-14841
40. Senarath, K., Payton, J. L., Kankanamge, D., Siripurapu, P., Tennakoon, M., and Karunarathne, A. (2018) $G\gamma$ identity dictates efficacy of $G\beta\gamma$ signaling and macrophage migration *J Biol Chem* **293**, 2974-2989
41. Tennakoon, M., Senarath, K., Kankanamge, D., Chadee, D. N., and Karunarathne, A. (2021) A short C-terminal peptide in $G\gamma$ regulates $G\beta\gamma$ signaling efficacy *Mol Biol Cell* **32**, 1446-1458
42. O'Neill, P. R., Karunarathne, W. K., Kalyanaraman, V., Silvius, J. R., and Gautam, N. (2012) G-protein signaling leverages subunit-dependent membrane affinity to differentially control $\beta\gamma$ translocation to intracellular membranes *Proc Natl Acad Sci U S A* **109**, E3568-3577
43. Prévost, M., Oliveira, I. T., Kocher, J.-P., and Wodak, S. J. (1996) Free Energy of Cavity Formation in Liquid Water and Hexane *The Journal of Physical Chemistry* **100**, 2738-2743
44. Zhu, C., Gao, Y., Li, H., Meng, S., Li, L., Francisco, J. S. *et al.* (2016) Characterizing hydrophobicity of amino acid side chains in a protein environment via measuring contact angle of a water nanodroplet on planar peptide network *Proc Natl Acad Sci U S A* **113**, 12946-12951
45. Kovacs, J. M., Mant, C. T., and Hodges, R. S. (2006) Determination of intrinsic hydrophilicity/hydrophobicity of amino acid side chains in peptides in the absence of nearest-neighbor or conformational effects *Biopolymers* **84**, 283-297
46. Guntas, G., Hallett, R. A., Zimmerman, S. P., Williams, T., Yumerefendi, H., Bear, J. E. *et al.* (2015) Engineering an improved light-induced dimer (iLID) for controlling the localization and activity of signaling proteins *Proc Natl Acad Sci U S A* **112**, 112-117
47. Hodges-Loaiza, H. B., Parker, L. E., and Cox, A. D. (2011) Prenylation and Phosphorylation of Ras Superfamily Small GTPases In Protein Prenylation Part B, Hrycyna CA, Bergo MO, Tamanoi F, eds. Academic Press, 43-69
48. Hancock, J. F., Cadwallader, K., Paterson, H., and Marshall, C. J. (1991) A CAAX or a CAAL motif and a second signal are sufficient for plasma membrane targeting of ras proteins *EMBO J* **10**, 4033-4039
49. Hancock, J. F., Paterson, H., and Marshall, C. J. (1990) A polybasic domain or palmitoylation is required in addition to the CAAX motif to localize p21ras to the plasma membrane *Cell* **63**, 133-139
50. Willumsen, B. M., Cox, A. D., Solski, P. A., Der, C. J., and Buss, J. E. (1996) Novel determinants of H-Ras plasma membrane localization and transformation *Oncogene* **13**, 1901-1909
51. Sokalingam, S., Raghunathan, G., Soundrarajan, N., and Lee, S. G. (2012) A study on the effect of surface lysine to arginine mutagenesis on protein stability and structure using green fluorescent protein *PLoS One* **7**
52. Cabrera-Vera, T. M., Vanhauwe, J., Thomas, T. O., Medkova, M., Preininger, A., Mazzoni, M. R. *et al.* (2003) Insights into G protein structure, function, and regulation *Endocr Rev* **24**, 765-781
53. Brunsveld, L., Waldmann, H., and Huster, D. (2009) Membrane binding of lipidated Ras peptides and proteins--the structural point of view *Biochim Biophys Acta* **1788**, 273-288

54. Ajith Karunarathne, W. K., O'Neill, P. R., Martinez-Espinosa, P. L., Kalyanaraman, V., and Gautam, N. (2012) All G protein $\beta\gamma$ complexes are capable of translocation on receptor activation *Biochem Biophys Res Commun* **421**, 605-611
55. Apolloni, A., Prior, I. A., Lindsay, M., Parton, R. G., and Hancock, J. F. (2000) H-ras but not K-ras traffics to the plasma membrane through the exocytic pathway *Mol Cell Biol* **20**, 2475-2487
56. Wedegaertner, P. B., Wilson, P. T., and Bourne, H. R. (1995) Lipid modifications of trimeric G proteins *J Biol Chem* **270**, 503-506
57. Takida, S., and Wedegaertner, P. B. (2003) Heterotrimer formation, together with isoprenylation, is required for plasma membrane targeting of G $\beta\gamma$ *J Biol Chem* **278**, 17284-17290
58. Saini, D. K., Kalyanaraman, V., Chisari, M., and Gautam, N. (2007) A family of G protein $\beta\gamma$ subunits translocate reversibly from the plasma membrane to endomembranes on receptor activation *J Biol Chem* **282**, 24099-24108
59. Akgoz, M., Kalyanaraman, V., and Gautam, N. (2004) Receptor-mediated reversible translocation of the G protein $\beta\gamma$ complex from the plasma membrane to the Golgi complex *J Biol Chem* **279**, 51541-51544
60. Masuho, I., Skamangas, N. K., Muntean, B. S., and Martemyanov, K. A. (2021) Diversity of the G $\beta\gamma$ complexes defines spatial and temporal bias of GPCR signaling *Cell Syst* **12**, 324-337
61. Arbuzova, A., Wang, L., Wang, J., Hangyas-Mihalyne, G., Murray, D., Honig, B. *et al.* (2000) Membrane binding of peptides containing both basic and aromatic residues. Experimental studies with peptides corresponding to the scaffolding region of caveolin and the effector region of MARCKS *Biochemistry* **39**, 10330-10339
62. Hurowitz, E. H., Melnyk, J. M., Chen, Y. J., Kouros-Mehr, H., Simon, M. I., and Shizuya, H. (2000) Genomic characterization of the human heterotrimeric G protein α , β , and γ subunit genes *DNA Res* **7**, 111-120
63. Cook, L. A., Schey, K. L., Cleator, J. H., Wilcox, M. D., Dingus, J., and Hildebrandt, J. D. (2001) Identification of a region in G protein γ subunits conserved across species but hypervariable among subunit isoforms *Protein Sci* **10**, 2548-2555
64. Choy, E., Chiu, V. K., Silletti, J., Feoktistov, M., Morimoto, T., Michaelson, D. *et al.* (1999) Endomembrane trafficking of ras: the CAAX motif targets proteins to the ER and Golgi *Cell* **98**, 69-80
65. Zhou, Y., Wong, C. O., Cho, K. J., van der Hoeven, D., Liang, H., Thakur, D. P. *et al.* (2015) SIGNAL TRANSDUCTION. Membrane potential modulates plasma membrane phospholipid dynamics and K-Ras signaling *Science* **349**, 873-876
66. Zhou, Y., Liang, H., Rodkey, T., Ariotti, N., Parton, R. G., and Hancock, J. F. (2014) Signal integration by lipid-mediated spatial cross talk between Ras nanoclusters *Mol Cell Biol* **34**, 862-876
67. Zhou, Y., Prakash, P., Liang, H., Cho, K. J., Gorfe, A. A., and Hancock, J. F. (2017) Lipid-Sorting Specificity Encoded in K-Ras Membrane Anchor Regulates Signal Output *Cell* **168**, 239-251
68. Uhlen, M., Fagerberg, L., Hallstrom, B. M., Lindskog, C., Oksvold, P., Mardinoglu, A. *et al.* (2015) Proteomics. Tissue-based map of the human proteome *Science* **347**, 1260419
69. Uhlen, M., Zhang, C., Lee, S., Sjostedt, E., Fagerberg, L., Bidkhori, G. *et al.* (2017) A pathology atlas of the human cancer transcriptome *Science* **357**

70. Thul, P. J., Akesson, L., Wiking, M., Mahdessian, D., Geladaki, A., Ait Blal, H. *et al.* (2017) A subcellular map of the human proteome *Science* **356**
71. Tennakoon, M., Senarath, K., Kankanamge, D., Ratnayake, K., Wijayaratna, D., Olupothage, K. *et al.* (2021) Subtype-dependent regulation of G $\beta\gamma$ signalling *Cell Signal* **82**, 109947
72. Simanshu, D. K., Nissley, D. V., and McCormick, F. (2017) RAS Proteins and Their Regulators in Human Disease *Cell* **170**, 17-33
73. Pylayeva-Gupta, Y., Grabocka, E., and Bar-Sagi, D. (2011) RAS oncogenes: weaving a tumorigenic web *Nat Rev Cancer* **11**, 761-774
74. Kankanamge, D., Tennakoon, M., Karunarathne, A., and Gautam, N. (2022) G protein γ subunit, a hidden master regulator of GPCR signaling *J Biol Chem* **298**, 102618
75. Vallar, L. (1996) Oncogenic role of heterotrimeric G proteins *Cancer Surv* **27**, 325-338
76. Henkels, K. M., Rehl, K. M., and Cho, K. J. (2021) Blocking K-Ras Interaction With the Plasma Membrane Is a Tractable Therapeutic Approach to Inhibit Oncogenic K-Ras Activity *Front Mol Biosci* **8**, 673096
77. Haney, S. L., and Holstein, S. A. (2023) Targeting the Isoprenoid Biosynthetic Pathway in Multiple Myeloma *International Journal of Molecular Sciences* **24**, 111,
78. Saini, D. K., Karunarathne, W. K., Angaswamy, N., Saini, D., Cho, J. H., Kalyanaraman, V. *et al.* (2010) Regulation of Golgi structure and secretion by receptor-induced G protein $\beta\gamma$ complex translocation *Proc Natl Acad Sci U S A* **107**, 11417-11422
79. Ratnayake, K., Kankanamge, D., Senarath, K., Siripurapu, P., Weis, N., Tennakoon, M. *et al.* (2017) Chapter 1 - Measurement of GPCR-G protein activity in living cells In *Methods in Cell Biology*, Shukla AK, ed. Academic Press, 1-25
80. Nedyalkova, M. A., Madurga, S., Tobiszewski, M., and Simeonov, V. (2019) Calculating the Partition Coefficients of Organic Solvents in Octanol/Water and Octanol/Air *J Chem Inf Model* **59**, 2257-2263 [10.1021/acs.jcim.9b00212](https://doi.org/10.1021/acs.jcim.9b00212)
81. Hattotuwegama, C. K., and Flower, D. R. (2006) Empirical prediction of peptide octanol-water partition coefficients *Bioinformatics* **1**, 257-259
82. Peverati, R., and Truhlar, D. G. (2011) Improving the Accuracy of Hybrid Meta-GGA Density Functionals by Range Separation *The Journal of Physical Chemistry Letters* **2**, 2810-2817
83. Marenich, A. V., Cramer, C. J., and Truhlar, D. G. (2009) Universal solvation model based on solute electron density and on a continuum model of the solvent defined by the bulk dielectric constant and atomic surface tensions *J Phys Chem B* **113**, 6378-6396
84. Frisch, M. J., Trucks, G. W., Schlegel, H. B., Scuseria, G. E., Robb, M. A., Cheeseman, J. R. *et al.* (2016) Gaussian 16 Rev. C.01 Wallingford, CT

Figure Legends

Figure 1. $G\gamma$ subtypes show differential sensitivities to statin-induced inhibition of membrane binding.

(A) Images of HeLa cells expressing YFP tagged $G\gamma$ 1-5 and 7-13 under the vehicle (control), Fluvastatin (20 μ M), FTI (1 μ M), or GGTI (10 μ M) treated conditions. Images represent the prominent phenotype observed in each population under the given experimental condition (scale: 5 μ m; $n \geq 15$ for each $G\gamma$ type). Whisker box plots generated using fluorescence recovery after half-cell photobleaching of the above cells show the variations in mobility half-time ($t_{1/2}$) of G protein heterotrimers containing different $G\gamma$ subtypes, with (B) control, (C) Fluvastatin-treated, (D) FTI-treated, and (E) GGTI-treated conditions (Average whisker box plots were plotted using mean \pm SD; Error bars: SD (Standard deviation); control: $n \geq 12$ cells for each $G\gamma$ from 154 cells, Fluvastatin-treated: $n \geq 10$ cells for each $G\gamma$ from 200 cells, FTI-treated: $n \geq 11$ cells for each $G\gamma$ from 132 cells, GGTI-treated: $n \geq 11$ cells for each $G\gamma$ 3 from 135 cells (each treatment was performed in $3 \leq$ independent experiments; Statistical comparisons were performed using One-way-ANOVA; $p < 0.05$; Flu: Fluvastatin; FTI: Farnesyl transferase inhibitor; GGTI: Geranylgeranyl transferase inhibitor).

Figure 2. Statin sensitivity and prenylation efficacy of $G\gamma$ are prenylation type independent.

(A) Subcellular distribution of GFP tagged wild type $G\gamma$ 9, $G\gamma$ 3, and mutants $G\gamma$ 9_{CALL}, and $G\gamma$ 3_{CIS}, with vehicle (control), Fluvastatin (20 μ M), FTI (1 μ M), or GGTI (10 μ M) treated conditions. Images represent the prominent phenotype observed in each population under the given experimental condition (scale: 5 μ m; $n \geq 15$ for each $G\gamma$ type). (B) Grouped box chart shows the percentages of cells in each $G\gamma$ type ($G\gamma$ 9 WT, $G\gamma$ 3 WT, $G\gamma$ 9_{CALL}, and $G\gamma$ 3_{CIS}) showing near-complete (black) and partial (red) cytosolic distribution with Fluvastatin treatment. (C) The whisker box plots show mobility half-time ($t_{1/2}$) of proteins in (A) determined using fluorescence recovery after half-cell photobleaching. (Average box plots were plotted using mean \pm SD; Error bars: SD (Standard deviation); $G\gamma$ 9 WT: $n = 571$ total number of cells from 7 independent experiments, $G\gamma$ 3 WT: $n = 597$ total number of cells from 7 independent experiments, $G\gamma$ 9_{CALL}: $n = 624$ total number of cells from 7 independent experiments, $G\gamma$ 3_{CIS}: $n = 408$ total number of cells from 5 independent experiments; Statistical comparisons were performed using One-way-ANOVA; $p < 0.05$; Flu: Fluvastatin; FTI: Farnesyl transferase inhibitor; GGTI: Geranylgeranyl transferase inhibitor; WT: wild-type).

Figure 3. The pre-prenylation sequence determines statin sensitivity and prenylation efficacy of $G\gamma$.

(A) Comparison of Ct domain amino acid sequences of $G\gamma$. The Ct domain of $G\gamma$ consists of the starting conserved NPF sequence, followed by the middle pre-CaaX region and the final CaaX motif. $G\gamma$ subtypes with a C-terminal *Ser* (Black) at the 'X' position are farnesylated. $G\gamma$ s containing *Leu* (light blue) at the 'X' position of CaaX are geranylgeranylated. During prenylation, the prenyl moiety is attached to the prenylated *Cys* (maroon), and this *Cys* is further modified during post-prenylation processing (proteolysis at the C-terminal three -aaX residues by the Ras converting CaaX endopeptidase 1 (RCE1), and then carboxymethylation of the new isoprenylcysteine C-terminus by isoprenylcysteine carboxyl methyltransferase (ICMT)). In the pre-CaaX region, hydrophobic *Phe* residues are shown in red, and positively charged

residues are in blue. **(B)** The scatter plot shows the log CE values to measure the hydrophobicity of pre-CaaX+CaaX Ct polypeptide regions of $G\gamma$. **(C)** Images of HeLa cells expressing GFP tagged $G\gamma 9$ -WT, $G\gamma 3$ -WT, $G\gamma 9_{G\gamma 3PC}$, and $G\gamma 3_{G\gamma 9PC}$, exposed to vehicle (Control), Fluvastatin (20 μ M), FTI (1 μ M), or GGTI (10 μ M). Images represent the prominent phenotype observed in each population under given experimental conditions (scale: 5 μ m; $n \geq 15$ for each $G\gamma$ type). **(D)** Grouped box chart shows the percentages of cells in each $G\gamma$ mutant ($G\gamma 9_{G\gamma 3PC}$, $G\gamma 3_{G\gamma 9PC}$, $G\gamma 9_{GG \rightarrow FF}$, and $G\gamma 3_{FF \rightarrow GG}$ mutants) showing near-complete (black) and partial (red) cytosolic distribution with Fluvastatin treatment. The black/red circles indicate the % cells showed near-complete or partial cytosolic distribution in each corresponding wild-type $G\gamma$ expressing cells. **(E)** The whisker box plots show mobility half-time ($t_{1/2}$) of proteins in (C) determined using fluorescence recovery after half-cell photobleaching. (Average box plots were plotted using mean \pm SD; Error bars: SD (Standard deviation); $G\gamma 9$ WT: $n = 571$ total number of cells from 7 independent experiments, $G\gamma 3$ WT: $n = 597$ total number of cells from 7 independent experiments, $G\gamma 9_{G\gamma 3PC}$: $n = 686$ total number of cells from 8 independent experiments, $G\gamma 3_{G\gamma 9PC}$: $n = 754$ total number of cells from 8 independent experiments; Statistical comparisons were performed using One-way-ANOVA; $p < 0.05$; Flu: Fluvastatin; FTI: Farnesyl transferase inhibitor; GGTI: Geranylgeranyl transferase inhibitor; PC: pre-CaaX).

Figure 4. Hydrophobic residues adjacent to prenylated Cys contribute significantly to the prenylation efficacy and statin sensitivity of $G\gamma$. **(A)** Comparison of Ct domain amino acid sequences of $G\gamma 3$ -WT and $G\gamma 9$ -WT. **(B)** Images of HeLa cells expressing GFP tagged $G\gamma 9_{GG \rightarrow FF}$, $G\gamma 3_{FF \rightarrow GG}$, $G\gamma 3_{FF \rightarrow LL}$, $G\gamma 3_{FF \rightarrow VV}$, $G\gamma 3_{FF \rightarrow YY}$, and $G\gamma 3_{FF \rightarrow AA}$ mutants exposed to vehicle (Control), Fluvastatin (20 μ M), FTI (1 μ M), or GGTI (10 μ M). Images represent the prominent phenotype observed in each population under given experimental conditions (scale: 5 μ m; $n \geq 15$ for each $G\gamma$ type). **(C)** Grouped box chart shows the percentages of cells in each $G\gamma$ mutant ($G\gamma 9_{GG \rightarrow FF}$, $G\gamma 3_{FF \rightarrow GG}$, $G\gamma 3_{FF \rightarrow LL}$, $G\gamma 3_{FF \rightarrow VV}$, $G\gamma 3_{FF \rightarrow YY}$, and $G\gamma 3_{FF \rightarrow AA}$) showing near-complete (black) and partial (red) cytosolic distribution with Fluvastatin treatment. The black/red open circles indicate the % cells with near-complete or partial cytosolic distribution in each corresponding wild-type $G\gamma$ ($G\gamma 3$ -WT) expressing cells. **(D)** The whisker box plots show mobility half-time ($t_{1/2}$) of proteins in (B) determined using fluorescence recovery after half-cell photobleaching. (Average box plots were plotted using mean \pm SD; Error bars: SD (Standard deviation); $G\gamma 9_{GG \rightarrow FF}$: $n = 884$ total number of cells from 9 independent experiments, $G\gamma 3_{FF \rightarrow GG}$: $n = 225$ total number of cells from 3 independent experiments, $G\gamma 3_{FF \rightarrow LL}$: $n = 428$ total number of cells, $G\gamma 3_{FF \rightarrow VV}$: $n = 364$ total number of cells, $G\gamma 3_{FF \rightarrow YY}$: $n = 407$ total number of cells, $G\gamma 3_{FF \rightarrow AA}$: $n = 358$ total number of cells; Each $G\gamma$ mutant was examined in 3 independent experiments; Statistical comparisons were performed using One-way-ANOVA; $p < 0.05$; Flu: Fluvastatin; FTI: Farnesyl transferase inhibitor; GGTI: Geranylgeranyl transferase inhibitor; WT: wild-type).

Figure 5. Optogenetic amino acid masking-unmasking shows pre-CaaX hydrophobicity-dependent prenylation efficacy and post-prenylation behavior regulation of proteins. **(A)** The modeled structures of the two photoswitches, iLID_{FCALL} and iLID_{GGGGFFCALL} (based on PDB ID-4WF0) before their prenylation. Resembling $G\gamma 3$ *Phe-duo*, the introduced *Phe550* (orange) in iLID_{FCALL} (Top) creates the *Phe-duo* using *Phe549* (pink) of iLID. As a control, an iLID variant

with an exposed *Phe-duo* (*Phe554* and *Phe555*-light orange) was generated by placing a linker sequence (GGGG-light orange loop region) between iLID and *Phe-duo* (FF) (iLID_{GGGGFFCALL}-Bottom). The introduced F550 in iLID_{FCALL} fits into a hydrophobic pocket on the surface of the per-arnt-sim (PAS) domain made up of I417, I428, F429, and Y508 (green), while in iLID_{GGGGFFCALL} F549 fits into this hydrophobic pocket allowing the *Phe-duo* to be exposed. **(B)** Optogenetic regulation of prenylated iLID_{FCgerger}^{-OMe}. Blue light-induced Ja helix relaxation results in iLID's SsrA peptide unmasking, exposing the *Phe-duo*, likely promoting membrane interaction of iLID_F by inserting the *Phe-duo* (F549 and F550) and the geranylgeranyl moiety into the hydrophobic tail region of the lipid bilayer. The magnified view shows the hydrophobic interactions of the F549 in iLID_{FCgerger}^{-OMe} with the hydrophobic pocket of the PAS domain before blue light irradiation. **(C)** Images of HeLa cells expressing Venus-iLID_{FCALL}, overnight blue light exposed Venus-iLID_{FCALL} or Venus-iLID_{GGGGFFCALL} (control) show the initial subcellular distribution of the proteins and their blue light-induced changes. In the control protein, the yellow arrow indicates the Golgi/endomembrane distribution of the constructs (Scale bar: 5 μm). The whisker box plots show the Golgi:Nucleus Venus fluorescence ratio under each condition (Average box plots were plotted using mean \pm SD; Error bars: SD (Standard deviation); Statistical comparisons were performed using One-way-ANOVA; $p < 0.05$) **(D)** The plot shows the reversible recruitment of iLID_{FCALL} to the Golgi upon blue light (error bars: SD, $10 < n$). **(E)** Images of HeLa cells expressing Venus-iLID_{FCALL} or Venus-iLID_{GGGGFFCALL} show a completely cytosolic distribution of the two proteins when the cells are exposed to GGTI, before and after blue light irradiation (10 μm). **(F)** 3-D images of blue light irradiated HeLa cells expressing Venus-iLID_{FCALL}, GalT-dsRed, and CFP-KDEL. Blue light-induced Golgi recruitment of Venus-iLID_{FCALL} is confirmed by its colocalization with the Golgi marker GalT-dsRed and non-overlapping distribution with the ER marker CFP-KDEL (Scale bar: 5 μm) (BL: Blue light; O/N BL: Overnight blue light; GGTI: Geranylgeranyl transferase inhibitor).

Figure 6. Positively charged pre-CaaX residues also contribute to $\text{G}\gamma$ prenylation efficacy and statin sensitivity. **(A)** Images of HeLa cells expressing GFP tagged $\text{G}\gamma^9_{\text{KEK-GG}\rightarrow\text{REK-GG}}$, $\text{G}\gamma^9_{\text{KEK-GG}\rightarrow\text{REK-KGG}}$, and $\text{G}\gamma^9_{\text{KEK-GG}\rightarrow\text{KEK-KFF}}$ mutants treated with vehicle (control), Fluvastatin (20 μM), FTI (1 μM), or GGTI (10 μM). Images represent the prominent phenotype observed in each population under given experimental conditions (scale: 5 μm ; $n \geq 15$ for each $\text{G}\gamma$ type). **(B)** Grouped box chart shows the percentages of cells in each $\text{G}\gamma$ mutant ($\text{G}\gamma^9_{\text{KEK-GG}\rightarrow\text{REK-GG}}$, $\text{G}\gamma^9_{\text{KEK-GG}\rightarrow\text{REK-KGG}}$, and $\text{G}\gamma^9_{\text{KEK-GG}\rightarrow\text{KEK-KFF}}$ mutants) showing near-complete (black) and partial (red) cytosolic distribution with Fluvastatin treatment. The black/red dotted circles indicate the % cells with near-complete or partial prenylation inhibition in wild-type $\text{G}\gamma^9$ expressing cells. **(C)** The whisker box plots show mobility half-time ($t_{1/2}$) of proteins in (A) determined using fluorescence recovery after half-cell photobleaching. (Average box plots were plotted using mean \pm SD; Error bars: SD (Standard deviation); $\text{G}\gamma^9_{\text{KEK-GG}\rightarrow\text{REK-GG}}$: $n = 397$ total number of cells from 5 independent experiments, $\text{G}\gamma^9_{\text{KEK-GG}\rightarrow\text{REK-KGG}}$: $n = 764$ total number of cells from 7 independent experiments, $\text{G}\gamma^9_{\text{KEK-GG}\rightarrow\text{KEK-KFF}}$: $n = 546$ total number of cells from 5 independent experiments; Statistical comparisons were performed using One-way-ANOVA; $p < 0.05$; Flu: Fluvastatin; FTI: Farnesyl transferase inhibitor; GGTI: Geranylgeranyl transferase inhibitor).

Tables

Table 1: Mobility properties of G γ types.

| G γ type | Ct Sequence | Mobility $t_{1/2}$ (s) | | | |
|------------------|----------------|------------------------|-------------|--------------|--------------|
| | | Control | Flu* | FTI* | GGTI* |
| G γ 1-WT | NPFKELKGGCVIS | 101 \pm 9 | 11 \pm 5 | 10 \pm 4 | 100 \pm 10 |
| G γ 2-WT | NPFREKKFFCAIL | 90 \pm 11 | 49 \pm 10 | 97 \pm 12 | 41 \pm 9 |
| G γ 3-WT | NPFREKKFFCAIL | 102 \pm 14 | 55 \pm 12 | 98 \pm 15 | 43 \pm 9 |
| G γ 4-WT | NPFREKKFFCTIL | 97 \pm 11 | 58 \pm 17 | 92 \pm 10 | 47 \pm 12 |
| G γ 5-WT | NPFRPQKV-CSFL | 101 \pm 9 | 17 \pm 8 | 97 \pm 12 | 14 \pm 4 |
| G γ 7-WT | NPFKDKKP-CIIL | 94 \pm 12 | 22 \pm 8 | 98 \pm 9 | 13 \pm 4 |
| G γ 8-WT | NPFRDKRLFCVIL | 105 \pm 9 | 55 \pm 11 | 100 \pm 10 | 42 \pm 8 |
| G γ 9-WT | NPFKE-KGGCIIS | 96 \pm 13 | 9 \pm 5 | 9 \pm 3 | 95 \pm 10 |
| G γ 10-WT | NPFREPRS-CAIL | 97 \pm 9 | 9 \pm 5 | 95 \pm 8 | 16 \pm 5 |
| G γ 11-WT | NPFKE-KGSCVIS | 97 \pm 7 | 9 \pm 5 | 10 \pm 4 | 96 \pm 10 |
| G γ 12-WT | NPFKDKKT-CIIL | 96 \pm 7 | 49 \pm 8 | 102 \pm 12 | 27 \pm 5 |
| G γ 13-WT | NPWVEKGGK-CTIL | 95 \pm 12 | 8 \pm 5 | 95 \pm 18 | 9 \pm 4 |

*Mobility $t_{1/2}$ of major phenotype

Table 2: Mobility properties of G γ mutants.

| G γ mutant | Ct Sequence | Mobility $t_{1/2}$ (s) | | | | |
|--|---------------|------------------------|--------------|-------------|--------------|--------------|
| | | Control | Flu-Complete | Flu-Partial | FTI* | GGTI* |
| G γ 9 _{CALL} | NPFKE-KGGCALL | 95 \pm 7 | 7 \pm 4 | - | 94 \pm 8 | 7 \pm 5 |
| G γ 3 _{CIIS} | NPFREKKFFCIIS | 102 \pm 10 | - | 53 \pm 10 | 15 \pm 4 | 95 \pm 10 |
| G γ 9 _{Gγ3PC} | NPFREKKFFCIIS | 101 \pm 10 | 10 \pm 5 | 31 \pm 10 | 11 \pm 4 | 99 \pm 15 |
| G γ 3 _{Gγ9PC} | NPFKE-KGGCAIL | 101 \pm 11 | 5 \pm 3 | 55 \pm 11 | 101 \pm 14 | 5 \pm 3 |
| G γ 9 _{GG\rightarrowFF} | NPFKE-KFFCIIS | 101 \pm 11 | 6 \pm 3 | 26 \pm 5 | 12 \pm 5 | 105 \pm 11 |
| G γ 3 _{FF\rightarrowGG} | NPFREKKGGCAIL | 98 \pm 12 | 5 \pm 2 | 31 \pm 9 | 94 \pm 10 | 10 \pm 4 |
| G γ 3 _{FF\rightarrowLL} | NPFREKKLLCAIL | 97 \pm 10 | 9 \pm 3 | 45 \pm 10 | 99 \pm 13 | 52 \pm 11 |
| G γ 3 _{FF\rightarrowVV} | NPFREKKVVCAIL | 103 \pm 13 | 7 \pm 6 | 28 \pm 8 | 93 \pm 11 | 9 \pm 7 |
| G γ 3 _{FF\rightarrowYY} | NPFREKKYYCAIL | 95 \pm 13 | 9 \pm 5 | 31 \pm 7 | 96 \pm 8 | 12 \pm 4 |
| G γ 3 _{FF\rightarrowAA} | NPFREKKAACAIL | 98 \pm 9 | 5 \pm 2 | 31 \pm 6 | 96 \pm 11 | 6 \pm 3 |
| G γ 9 _{KEK-GG\rightarrowREK-GG} | NPFRE-KGGCIIS | 101 \pm 17 | 12 \pm 6 | 45 \pm 8 | 7 \pm 4 | 95 \pm 10 |
| G γ 9 _{KEK-GG\rightarrowREKGG} | NPFREKKGGCIIS | 98 \pm 11 | 6 \pm 5 | 47 \pm 14 | 11 \pm 4 | 99 \pm 9 |
| G γ 9 _{KEK-GG\rightarrowKEKKFF} | NPFKEKKFFCIIS | 94 \pm 11 | 4 \pm 1 | 25 \pm 4 | 10 \pm 5 | 100 \pm 8 |
| G γ 3 _{F70G} | NPFREKKGFCAIL | 104 \pm 12 | 12 \pm 3 | 38 \pm 6 | 103 \pm 11 | 17 \pm 4 |
| G γ 3 _{F71G} | NPFREKKFGCAIL | 100 \pm 10 | 13 \pm 3 | 40 \pm 8 | 100 \pm 9 | 18 \pm 5 |

* Mobility $t_{1/2}$ of major phenotype

Table 3: Fluvastatin-induced prenylation inhibition (or partial inhibition) of G γ 3, G γ 9 and their Ct mutants.

| G γ mutant | Ct Sequence | Percent cells (%) | |
|--|-----------------|-------------------|-----------------|
| | | Complete | Partial |
| G γ 9-WT | NPFKE - KGGCIIS | 99.7 \pm 0.5 | 0 |
| G γ 3-WT | NPFREKKFFCAIL | 0 | 98.7 \pm 1.2 |
| G γ 9 ^{CALL} | NPFKE - KGGCALL | 98.6 \pm 1.2 | 0 |
| G γ 3 ^{CIIS} | NPFREKKFFCIIS | 2.9 \pm 0.7 | 97.1 \pm 0.7 |
| G γ 9 ^{Gγ3PC} | NPFREKKFFCIIS | 23.8 \pm 12.9 | 74.5 \pm 13.4 |
| G γ 3 ^{Gγ9PC} | NPFKE - KGGCAIL | 99.3 \pm 0.9 | 0 |
| G γ 9 ^{GG\rightarrowFF} | NPFKE - KFFCIIS | 87.4 \pm 2.7 | 12.5 \pm 2.7 |
| G γ 3 ^{FF\rightarrowGG} | NPFREKKGGCAIL | 94.5 \pm 1.3 | 5.5 \pm 1.3 |
| G γ 3 ^{FF\rightarrowLL} | NPFREKKLLCAIL | 4.1 \pm 3.1 | 95.9 \pm 3.1 |
| G γ 3 ^{FF\rightarrowVV} | NPFREKKVVCAIL | 88.2 \pm 4.5 | 11.8 \pm 4.5 |
| G γ 3 ^{FF\rightarrowYY} | NPFREKKYYCAIL | 87.9 \pm 2.3 | 12.1 \pm 2.3 |
| G γ 3 ^{FF\rightarrowAA} | NPFREKKAACAIL | 92.8 \pm 3.0 | 7.2 \pm 3.0 |
| G γ 9 ^{KEK-GG\rightarrowREK-GG} | NPFRE - KGGCIIS | 83.6 \pm 1.6 | 15.7 \pm 0.7 |
| G γ 9 ^{KEK-GG\rightarrowREKGG} | NPFREKKGGCIIS | 65.2 \pm 3.8 | 35.7 \pm 5.9 |
| G γ 9 ^{KEK-GG\rightarrowKEKKFF} | NPFKEKKFFCIIS | 51.3 \pm 6.3 | 48.5 \pm 6.4 |
| G γ 3 ^{F70G} | NPFREKKGFCAIL | 28.9 \pm 1.1 | 72.6 \pm 0.9 |
| G γ 3 ^{F71G} | NPFREKKFGCAIL | 20.0 \pm 0.4 | 77.7 \pm 5.6 |

Figure 1

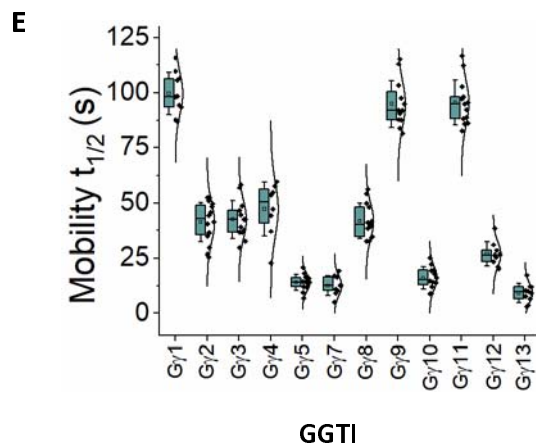
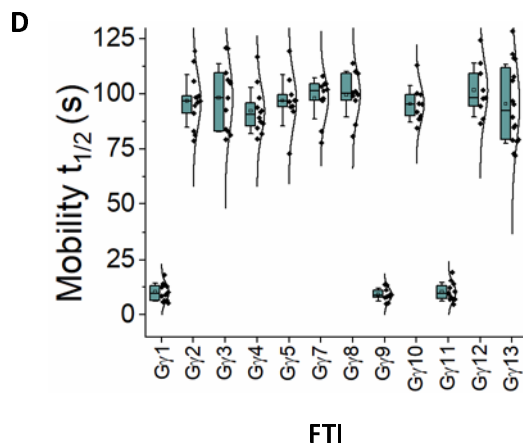
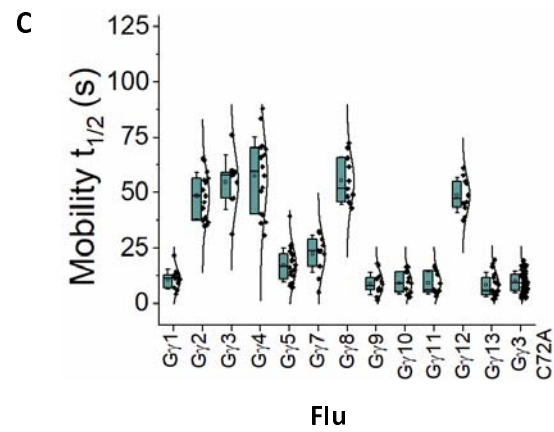
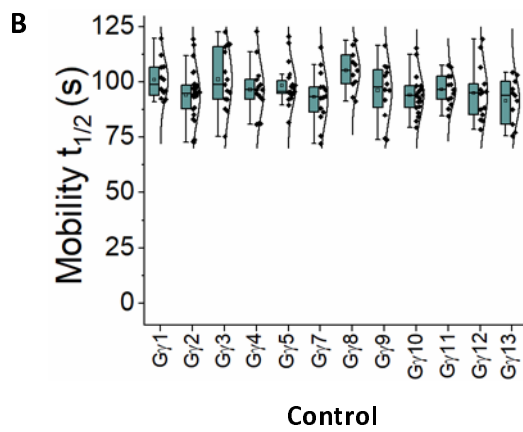
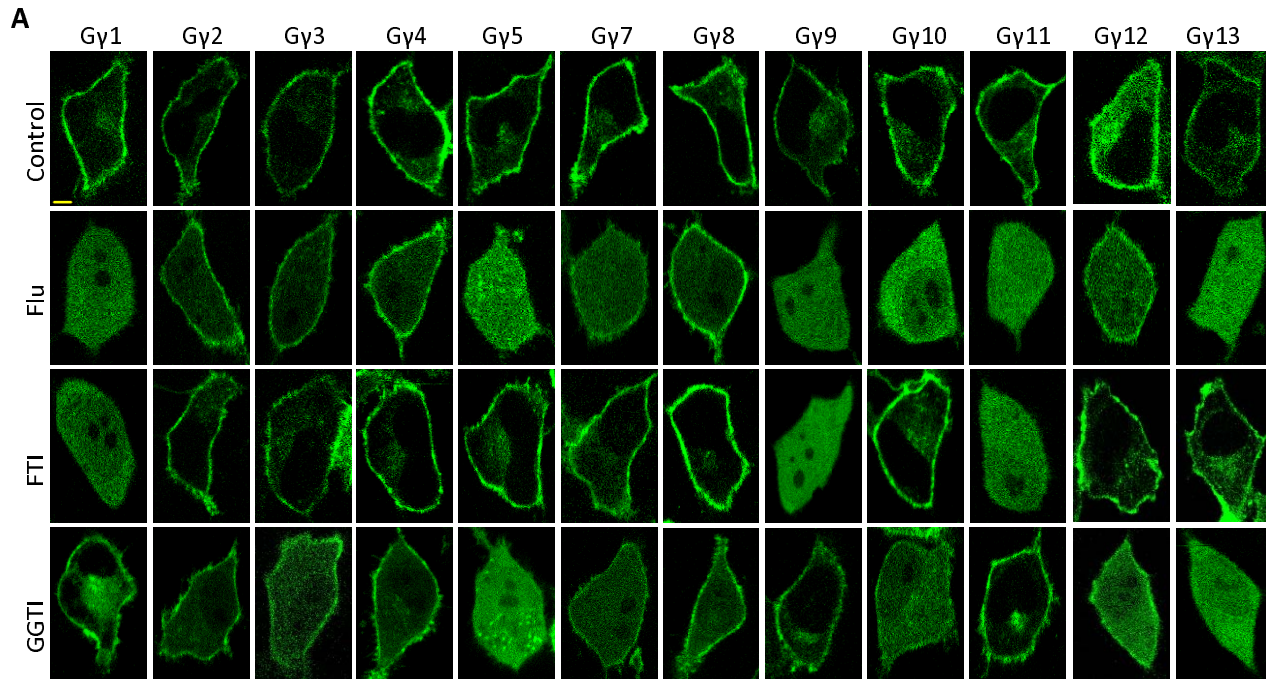


Figure 2

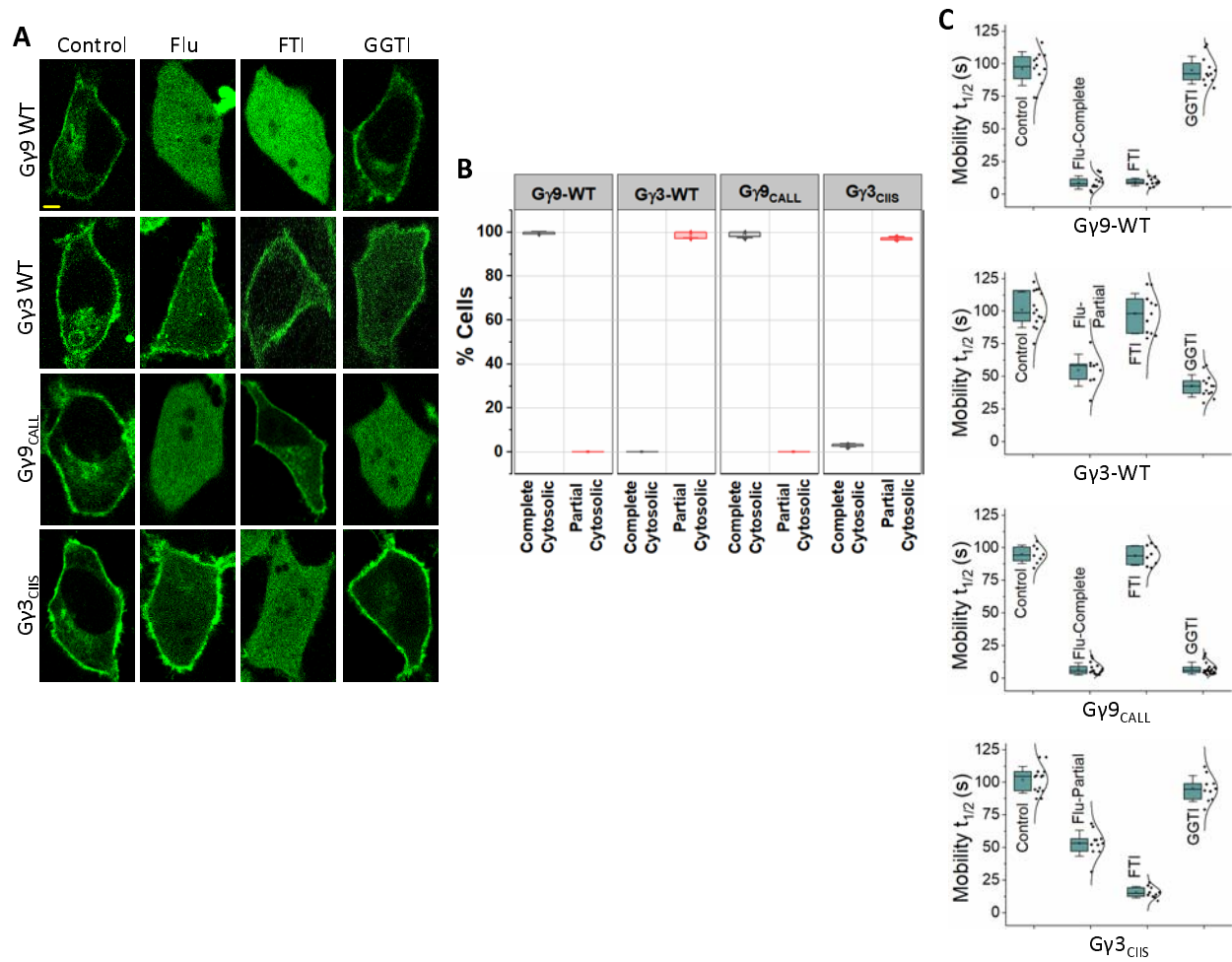


Figure 3

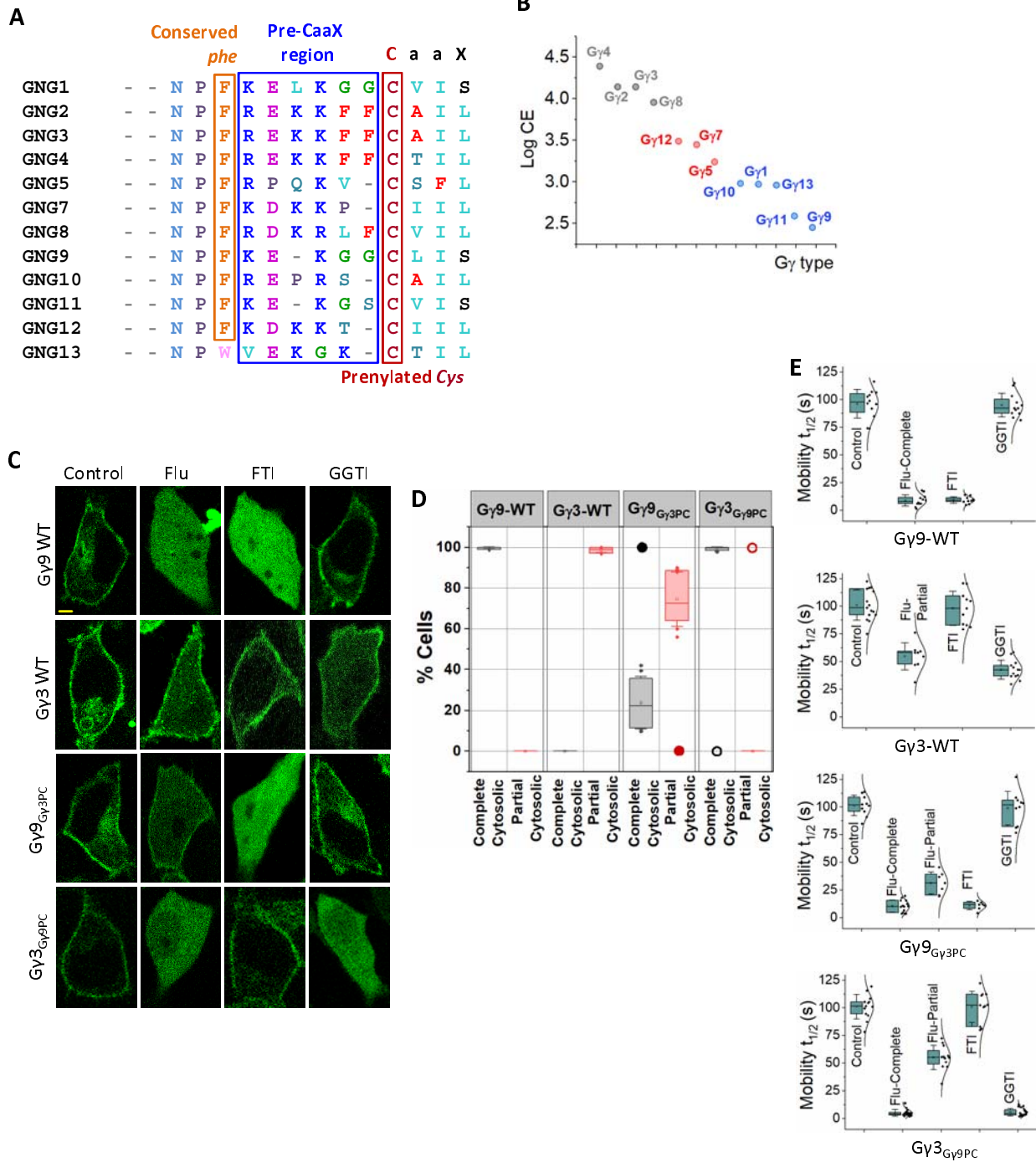


Figure 4

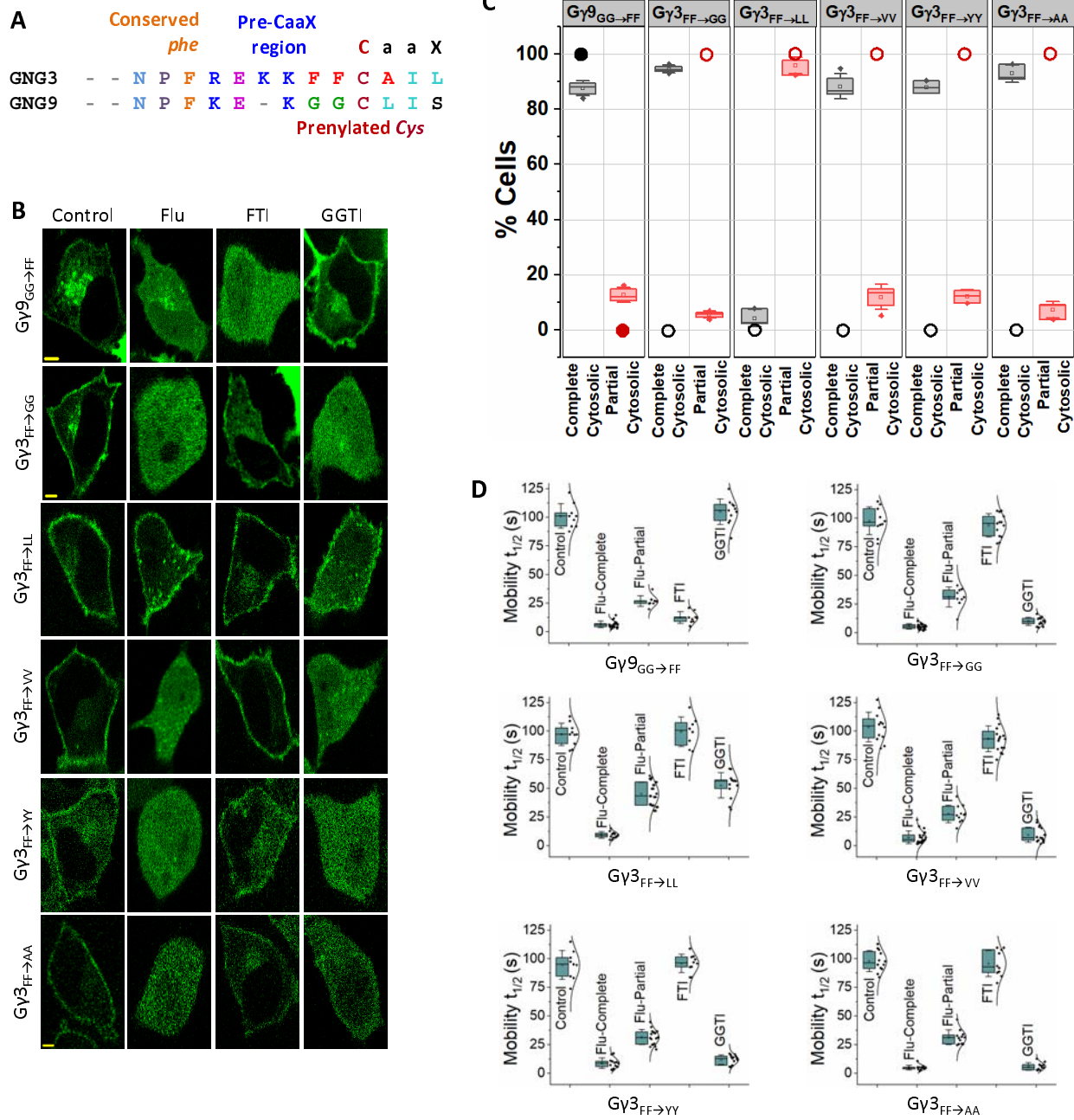


Figure 5

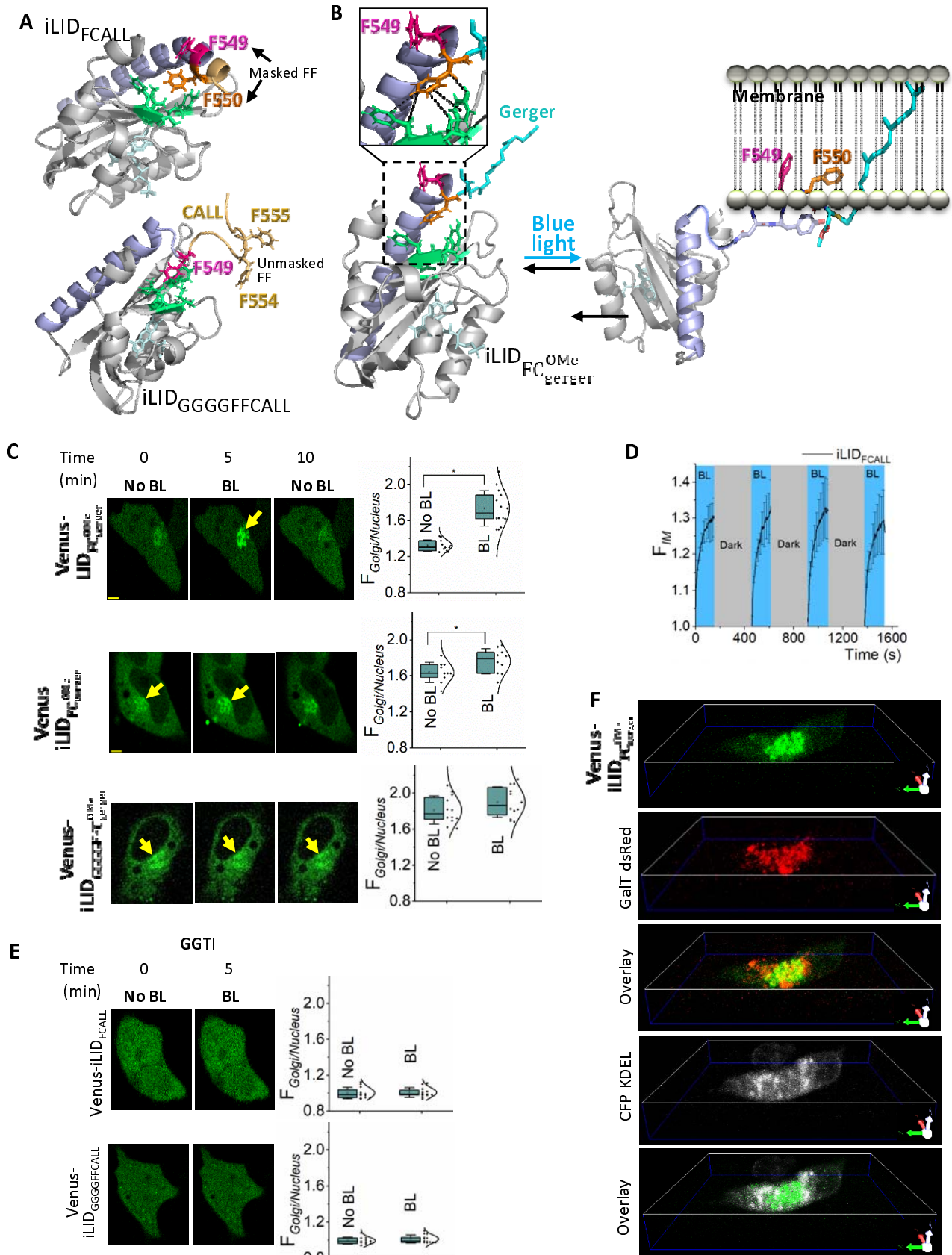


Figure 6

